INTERNATIONAL JOURNAL FOR NUMERICAL METHODS IN ENGINEERING
Int. J. Numer. Meth. Engng 2008; **74**:1128–1161
Published online 8 October 2007 in Wiley InterScience (www.interscience.wiley.com). DOI: 10.1002/nme.2204

Upper bound solution to elasticity problems: A unique property of the linearly conforming point interpolation method (LC-PIM)

G. R. Liu[1, 2, *, †] and G. Y. Zhang[1,2]

[1]*Centre for Advanced Computations in Engineering Science (ACES), Department of Mechanical Engineering, National University of Singapore, 9 Engineering Drive 1, 117576, Singapore*
[2]*The Singapore-MIT Alliance (SMA), E4-04-10, 4 Engineering Drive 3, 117576, Singapore*

SUMMARY

It is well known that the displacement-based fully compatible finite element method (FEM) provides a lower bound in energy norm for the exact solution to elasticity problems. It is, however, much more difficult to bound the solution from above for general problems in elasticity, and it has been a dream of many decades to find a systematical way to obtain such an upper bound. This paper presents a very important and unique property of the linearly conforming point interpolation method (LC-PIM): it provides a general means to obtain an upper bound solution in energy norm for elasticity problems. This paper conducts first a thorough theoretical study on the LC-PIM: we derive its weak form based on variational principles, study a number of properties of the LC-PIM, and prove that LC-PIM is variationally consistent and that it produces upper bound solutions. We then demonstrate these properties through intensive numerical studies with many examples of 1D, 2D, and 3D problems. Using the LC-PIM together with the FEM, we now have a systematical way to numerically obtain both upper and lower bounds of the exact solution to elasticity problems, as shown in these example problems. Copyright © 2007 John Wiley & Sons, Ltd.

Received 5 February 2007; Revised 16 July 2007; Accepted 29 August 2007

KEY WORDS: numerical methods; mesh-free methods; point interpolation method; nodal integration; solution bound; elasticity

1. INTRODUCTION

Mesh-free methods have been developed and achieved remarkable progress in recent years. Typical methods include the smooth particle hydrodynamic method [1, 2], the diffuse element

*Correspondence to: G. R. Liu, Centre for Advanced Computations in Engineering Science (ACES), Department of Mechanical Engineering, National University of Singapore, 9 Engineering Drive 1, 117576, Singapore.
†E-mail: mpeliugr@nus.edu.sg

method [3], the element-free Galerkin method [4], the reproducing kernel particle methods [5], the meshless local Petrov–Galerkin method [6], the point interpolation method (PIM) [7, 8], etc. A very detailed introduction on many types of mesh-free methods for different problems can be found in books by Liu [9] and Liu and Gu [10]. These methods have been shown to be effective for different classes of problems, have provided us many numerical techniques, and have extended our minds in the quest for more effective and robust computational methods.

The linearly conforming point interpolation method (LC-PIM) was evolved from the mesh-free PIM, which was originally formulated based on the Galerkin weak form with shape functions constructed using point interpolation procedure and a small set of nodes located in a local support domain. Two types of basis functions have been used in the PIM, i.e. polynomial basis functions [7] and radial basis functions (RBFs) [8, 11]. The unique feature of PIM is that the shape functions possess Delta function property, which allows straightforward imposition of point essential boundary conditions. Using the nodal integration scheme proposed by Chen *et al*. [12], Liu *et al*. have developed the linearly conforming radial point interpolation method (LC-RPIM) [13] and the LC-PIM [14, 15]. Both the LC-RPIM and the LC-PIM can guarantee linear exactness and monotonic convergence of the numerical solutions. Compared with the linear finite element method (FEM), the LC-PIM can obtain better accuracy and achieve higher convergence rate, especially for stress calculation [14].

The FEM has been used most widely for engineering problems [16, 17]. It is well known that the displacement-based fully compatible FEM provides a lower bound in energy norm for the exact solution to elasticity problems. It is, however, much more difficult to bound the solution from above for these problems, and it has been a dream of many decades to find a systematical way to obtain an upper bound of the exact solution. This paper presents a very important property of the LC-PIM: it provides an upper bound solution in energy norm for elasticity problems with homogeneous essential boundary conditions. We first derive the weak form for the LC-PIM based on the generalized two-field variational principle. We then prove that the LC-PIM is variationally consistent, and it possesses a number of properties including the important upper bound property. Finally, we demonstrate these properties through a number of numerical examples of one-dimensional (1D), 2D, and 3D problems. Using the LC-PIM together with the FEM, we now have a systematical way to numerically obtain both upper and lower bounds of the exact solution to elasticity problems, as shown in these wide ranges of example problems.

The formulation in this paper will largely be for 2D problems for the convenience of the presentation and without loss of generality. The extension of these formulae to 3D problems and reduction of those to 1D are straightforward and have already been implemented in our LC-PIM codes to analyze 1D, 2D, and 3D example problems that will be presented in this paper.

2. BASIC EQUATION FOR LINEARLY ELASTICITY PROBLEMS

Consider a 2D static elasticity problem governed by the equilibrium equation in the domain Ω bounded by Γ ($\Gamma=\Gamma_u+\Gamma_t; \Gamma_u\cap\Gamma_t=0$) as

$$\mathbf{L}_d^{\mathrm{T}}\boldsymbol{\sigma}+\mathbf{b}=0 \quad \text{in } \Omega \tag{1}$$

DOI: 10.1002/nme

where $\mathbf{L}_d$ is a matrix of differential operator defined as

$$\mathbf{L}_d = \begin{bmatrix} \dfrac{\partial}{\partial x} & 0 \\ 0 & \dfrac{\partial}{\partial y} \\ \dfrac{\partial}{\partial y} & \dfrac{\partial}{\partial x} \end{bmatrix} \tag{2}$$

$\boldsymbol{\sigma}^{\mathrm{T}} = \{\sigma_{xx}\ \sigma_{yy}\ \tau_{xy}\}$ is the vector of stresses, and $\mathbf{b}^{\mathrm{T}} = \{b_x\ b_y\}$ is the vector of body force applied in the problem domain. The stresses relate the strains *via* the generalized Hook's law:

$$\boldsymbol{\sigma} = \mathbf{D}\boldsymbol{\varepsilon} \tag{3}$$

where $\mathbf{D}$ is the matrix of material constants, and $\boldsymbol{\varepsilon}^{\mathrm{T}} = \{\varepsilon_{xx}\ \varepsilon_{yy}\ \gamma_{xy}\}$ is the vector of strains given by

$$\boldsymbol{\varepsilon} = \mathbf{L}_d \mathbf{u} \tag{4}$$

where $\mathbf{u}$ is the displacement field. Boundary conditions are given as follows.

Essential (or displacement) boundary conditions:

$$\mathbf{u} = \hat{\mathbf{u}} \quad \text{on } \Gamma_u \tag{5}$$

where $\mathbf{u} = \{u_x\ u_y\}^{\mathrm{T}}$ is the vector of the displacement and $\hat{\mathbf{u}}$ is the vector of the prescribed displacements on the essential boundary Γ_u.

Natural (stress) boundary conditions:

$$\mathbf{L}_n^{\mathrm{T}} \boldsymbol{\sigma} = \hat{\mathbf{t}} \quad \text{on } \Gamma_t \tag{6}$$

where $\hat{\mathbf{t}}$ is the vector of the prescribed traction on the natural boundary Γ_t, and $\mathbf{L}_n^{\mathrm{T}}$ is the matrix of unit outward normal which can be expressed as

$$\mathbf{L}_n = \begin{bmatrix} n_x & 0 \\ 0 & n_y \\ n_y & n_x \end{bmatrix} \tag{7}$$

3. BRIEFING ON THE FEM

3.1. Basic formulation

For more effective discussion, we first brief on the standard formulation of FEM [16, 17], as some of these formulae will be used repetitively in later sections. In the FEM, compatible displacement fields are assumed, and a discrete set of algebraic equations of FEM are generated using the following energy functional:

$$J(\mathbf{u}) = \int_\Omega \boldsymbol{\varepsilon}^{\mathrm{T}} \mathbf{D}\boldsymbol{\varepsilon}\, \mathrm{d}\Omega - \int_\Omega \mathbf{u}^{\mathrm{T}} \mathbf{b}\, \mathrm{d}\Omega - \int_{\Gamma_t} \mathbf{u}^{\mathrm{T}} \hat{\mathbf{t}}\, \mathrm{d}\Gamma \tag{8}$$

DOI: 10.1002/nme

where $\boldsymbol{\varepsilon}$ is the stain obtained using Equation (4), and $\mathbf{u} \in H^1(\Omega)$ are trial functions with corresponding test function of $\delta\mathbf{u} \in H_0^1(\Omega)$. Here, $H^1(\Omega)$ denotes the Sobolev space of functions with square integrable derivatives in Ω, and $H_0^1(\Omega)$ is the sub-set of $H^1(\Omega)$ that satisfies Equation (5). In the numerical implementations, the FEM divides the domain Ω into a number of elements, and the following trial functions are used:

$$\tilde{\mathbf{u}}(\mathbf{x}, \mathbf{d}) = \sum_{i \in n_e} \boldsymbol{\Phi}_i(\mathbf{x}) \mathbf{d}_i \tag{9}$$

where n_e is the set of nodes of the element containing $\mathbf{x}$, $\mathbf{d}_i = [u_{xi} \; u_{yi}]^{\mathrm{T}}$ is the vector of nodal displacements, and $\boldsymbol{\Phi}$ is a matrix of shape functions:

$$\boldsymbol{\Phi}_i(\mathbf{x}) = \begin{bmatrix} \varphi_i(\mathbf{x}) & 0 \\ 0 & \varphi_i(\mathbf{x}) \end{bmatrix} \tag{10}$$

in which $\varphi_i(\mathbf{x})$ is the shape function for node i. Using Equations (4) and (9), the strain of FEM approximation is given by

$$\tilde{\boldsymbol{\varepsilon}}(\mathbf{x}, \mathbf{d}) = \mathbf{L}_d \tilde{\mathbf{u}}(\mathbf{x}, \mathbf{d}) = \sum_{i \in n_e} \underbrace{\mathbf{L}_d \boldsymbol{\Phi}_i(\mathbf{x})}_{\tilde{\mathbf{B}}_i} \mathbf{d}_i = \sum_{i \in n_e} \tilde{\mathbf{B}}_i \mathbf{d}_i \tag{11}$$

with the *strain matrix* of FEM defined as

$$\tilde{\mathbf{B}}_i(\mathbf{x}) = \mathbf{L}_d \boldsymbol{\Phi}_i(\mathbf{x}) = \begin{bmatrix} \dfrac{\partial \varphi_i(\mathbf{x})}{\partial x} & 0 \\ 0 & \dfrac{\partial \varphi_i(\mathbf{x})}{\partial y} \\ \dfrac{\partial \varphi_i(\mathbf{x})}{\partial y} & \dfrac{\partial \varphi_i(\mathbf{x})}{\partial x} \end{bmatrix} \tag{12}$$

The stationary conditions of functional J defined by Equation (8) give the following *standard* Galerkin weak form:

$$\delta J(\mathbf{u}) = \int_\Omega (\delta\boldsymbol{\varepsilon})^{\mathrm{T}} \mathbf{D}\boldsymbol{\varepsilon} \, \mathrm{d}\Omega - \int_\Omega (\delta\mathbf{u})^{\mathrm{T}} \mathbf{b} \, \mathrm{d}\Omega - \int_{\Gamma_t} (\delta\mathbf{u})^{\mathrm{T}} \hat{\mathbf{t}} \, \mathrm{d}\Gamma = 0 \tag{13}$$

By substituting the approximations $\tilde{\mathbf{u}}$ into Equation (13) and invoking the arbitrariness of virtual nodal displacements, we have the standard discretized algebraic system equation:

$$\tilde{\mathbf{K}}\tilde{\mathbf{d}} = \tilde{\mathbf{f}} \tag{14}$$

where $\tilde{\mathbf{d}}$ is the vector of nodal displacement of FEM at all the unconstrained nodes, $\tilde{\mathbf{K}}$ is the (global) stiffness matrix of FEM that is assembled using

$$\tilde{\mathbf{K}}_{ij} = \int_\Omega \tilde{\mathbf{B}}_i^{\mathrm{T}} \mathbf{D} \tilde{\mathbf{B}}_j \, \mathrm{d}\Omega \tag{15}$$

and $\tilde{\mathbf{f}}$ is the vector of nodal forces at the unconstrained nodes that is assembled using

$$\tilde{\mathbf{f}}_i = \int_\Omega \boldsymbol{\Phi}_i^{\mathrm{T}}(\mathbf{x}) \mathbf{b} \, \mathrm{d}\Omega + \int_{\Gamma_t} \boldsymbol{\Phi}_i^{\mathrm{T}}(\mathbf{x}) \hat{\mathbf{t}} \, \mathrm{d}\Gamma \tag{16}$$

DOI: 10.1002/nme

3.2. Some properties of FEM

Now we state the following important properties of compatible FEM models, as these properties will be used in this work.

Remark 1 (*Lower bound property*)
The strain energy obtained from the FEM solution based on assumed displacements that are fully compatible is a lower bound of the exact strain energy. This property can be shown as follows

The strain energy obtained from the FEM solution can be expressed as

$$\tilde{U}(\tilde{\mathbf{d}}) = \int_{\Omega} \frac{1}{2} \tilde{\boldsymbol{\varepsilon}}^{\mathrm{T}} \mathbf{D} \tilde{\boldsymbol{\varepsilon}} \, \mathrm{d}\Omega = \frac{1}{2} \tilde{\mathbf{d}}^{\mathrm{T}} \tilde{\mathbf{K}} \tilde{\mathbf{d}} \tag{17}$$

Let the *exact* strain energy be defined as

$$U_0 = \int_{\Omega} \frac{1}{2} \boldsymbol{\varepsilon}_0^{\mathrm{T}} \mathbf{D} \boldsymbol{\varepsilon}_0 \, \mathrm{d}\Omega \tag{18}$$

where $\boldsymbol{\varepsilon}_0$ is the exact solution of strains of the problem, which relates to the exact solution of displacement $\mathbf{u}_0$ in the form of $\boldsymbol{\varepsilon}_0 = \mathbf{L}_d \mathbf{u}_0$. The exact solution satisfies all the equations given in Section 2: Equations (1)–(7).

For an FEM solution from solving Equation (14) based on assumed displacement that is fully *compatible*, the total potential energy at the stationary point can be expressed as

$$\tilde{J}(\tilde{\mathbf{d}}) = \tfrac{1}{2} \tilde{\mathbf{d}}^{\mathrm{T}} \tilde{\mathbf{K}} \tilde{\mathbf{d}} - \tilde{\mathbf{d}}^{\mathrm{T}} \underbrace{\tilde{\mathbf{f}}}_{\tilde{\mathbf{K}}\tilde{\mathbf{d}}} = -\tfrac{1}{2} \tilde{\mathbf{d}}^{\mathrm{T}} \tilde{\mathbf{K}} \tilde{\mathbf{d}} = -\tilde{U}(\tilde{\mathbf{d}}) \tag{19}$$

As the FEM solution of a compatible model is based on the minimum total potential energy principle, we have

$$\tilde{J} = -\tilde{U} \geqslant J_0 = -U_0 \tag{20}$$

or

$$\tilde{U}(\tilde{\boldsymbol{\varepsilon}}) \leqslant U_0(\boldsymbol{\varepsilon}_0) \tag{21}$$

which means that the strain energy obtained from an FEM solution is a lower bound of the exact solution of strain energy.

Remark 1 implies that the strain energy obtained from the displacement-based fully compatible FEM solution is always an underestimate of the exact strain energy, and the displacement is always a lower bound of the exact solution in the 'K norm' (or strain energy). Similar discussions on the lower bound property of FEM can be found in [16].

The above-mentioned lower bound property of FEM is valid for all types of elements as long as the displacement field is compatible. In this work, however, we use only linear triangular elements (that is compatible) when FEM is used.

Remark 2 (*Monotonic property*)
For given a sequence of n_m meshes $M_1, M_2, \ldots, M_{n_m}$, in which the nodes in M_i contain that in M_{i-1} $(i = 2, 3, \ldots, n_m)$, the following inequalities then stand:

$$\tilde{U}(\tilde{\boldsymbol{\varepsilon}}_{M_1}) \leqslant \tilde{U}(\tilde{\boldsymbol{\varepsilon}}_{M_2}) \leqslant \cdots \leqslant \tilde{U}(\tilde{\boldsymbol{\varepsilon}}_{M_{n_m}}) \leqslant U_0(\boldsymbol{\varepsilon}_0) \tag{22}$$

DOI: 10.1002/nme

where $\tilde{\boldsymbol{\varepsilon}}_{M_i}$ is the FEM compatible solution of strains obtained using mesh M_i. This property can be shown easily using the arguments given by Oliveira [18].

Remark 3 (*Reproducibility property*)
If the exact solution lives in the space of the shape functions used in Equation (9), the FEM solution of compatible model will be exact.

This property of FEM can be shown easily using the arguments given in Oliveira [18] and Liu and Quek [17].

4. BRIEFING ON THE LINEARLY CONFORMING POINT INTERPOLATION METHOD (LC-PIM)

Detailed formulations of the LC-PIM have been proposed in the previous work [14]. Here, we briefly introduce the basic procedures and expressions in the following section.

4.1. Construction of PIM shape functions

In the LC-PIM, the displacements are assumed using Equation (9) and shape functions that are generally constructed using the PIM with a small group of nodes in the local support domain of a point of interest. The general procedure of constructing shape functions using both polynomial functions and RBFs can be found in the mesh-free method book by Liu [9]. In the simplest setting of the LC-PIM, background cells of 3-node triangles are employed for the construction of shape functions. Both linear and quadratic interpolation procedures are implemented in the LC-PIM in our previous works [14]. When linear interpolation is used, the procedure is basically the same as that in the conventional FEM using linear triangular elements. In quadratic interpolations, background cells have been classified into two groups: interior and edge cells. An interior cell is a cell that has no edge on the boundary of the problem domain and an edge cell is a cell that has at least one edge on the boundary of the problem domain. Then the point of interest located in an edge cell will be approximated linearly using the three vertexes of the cell and a point located in an interior cell will be approximated using six nodes including the vertexes of this cell and other three vertexes of the neighboring cells [14]. The LC-PIM using linear shape function for interpolation is very efficient and even more efficient compared with the conventional FEM using linear triangular elements [14]. The formulation is also very easy to follow. In the present work, therefore, we focus on the use of the simplest linear interpolation, which means we use exactly these same interpolations as in the FEM using linear triangular elements. After the theorems are proven and well understood, we will then extend them to general cases.

4.2. Discretized system equations

In the LC-PIM, any assumed displacement $\mathbf{u}$ and the corresponding assumed strains $\widehat{\boldsymbol{\varepsilon}}(\mathbf{u})$ satisfy the *generalized* Galerkin weak form that can be expressed as

$$\int_{\Omega} \delta(\widehat{\boldsymbol{\varepsilon}}(\mathbf{u}))^{\mathrm{T}} \mathbf{D}(\widehat{\boldsymbol{\varepsilon}}(\mathbf{u}))\,\mathrm{d}\Omega - \int_{\Omega} \delta\mathbf{u}^{\mathrm{T}}\mathbf{b}\,\mathrm{d}\Omega - \int_{\Gamma_t} \delta\mathbf{u}^{\mathrm{T}}\hat{\mathbf{t}}\,\mathrm{d}\Gamma = 0 \tag{23}$$

The overall procedure of the LC-PIM is as follows. We first assume that the displacement is approximated using Equation (9), which implies that the displacement at any point in the problem

DOI: 10.1002/nme

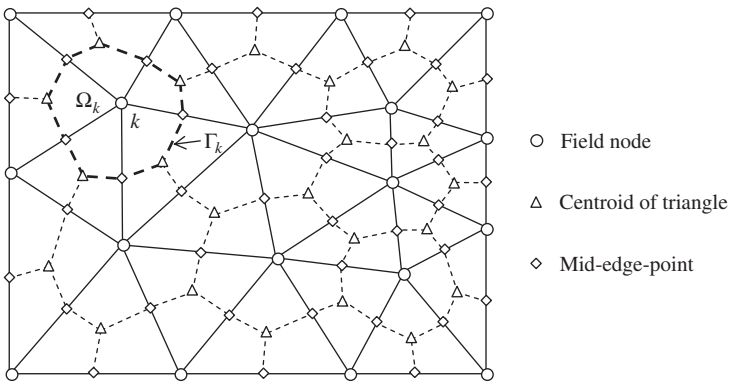

Figure 1. Illustration of background triangular cells and the smoothing domain created by sequentially connecting the centroids with the mid-edge points of the surrounding triangles of a node.

domain is interpolated using the PIM shape functions created using the nodes in the support domain of the point. We then assume the strain field using the assumed displacement field for each of the node; hence the strain is *not* independent of the displacement. The strain energy (corresponding to the first term in Equation (23)) in the problem domain is then calculated using the assumed strain, which is constant in a smoothing domain. A set of discretized algebraic system equation can be obtained in the following matrix form:

$$\widehat{\mathbf{K}}\,\widehat{\mathbf{d}} = \widehat{\mathbf{f}} \tag{24}$$

In obtaining Equation (24), integrations over the problem domain Ω need to be performed based on nodes. The detailed procedure leading to Equation (24) is given in the following sub-section.

For the convenience in our derivation, we first use the same set of shape functions for both FEM and LC-PIM; therefore, the assumed displacement in LC-PIM is also $\tilde{\mathbf{u}}$ defined in Equation (9), and $\tilde{\mathbf{f}}$ and $\widehat{\mathbf{f}}$ are also the same. In the following we will thus make no difference between $\tilde{\mathbf{f}}$ and $\widehat{\mathbf{f}}$. Note that the resultant strains $\tilde{\boldsymbol{\varepsilon}}$ in FEM and the assumed strains $\widehat{\boldsymbol{\varepsilon}}$ in LC-PIM are different, and so are the solutions of the nodal displacements for FEM $\tilde{\mathbf{d}}$ and that of LC-PIM $\widehat{\mathbf{d}}$.

4.3. Nodal integration scheme with strain smoothing operation

In the LC-PIM, the integration required in the weak form Equation (23) is performed based on the nodes in the problem domain, and a stabilized nodal integration scheme [12] is used in the LC-PIM. In such a nodal integration process, the problem domain Ω is divided into smoothing domains $\Omega = \Omega_1 \cup \Omega_2 \cup \cdots \cup \Omega_N$ and $\Omega_i \cap \Omega_j = \varnothing, i \neq j$, where N is the number of total field nodes located in the entire problem domain. The smoothing domain Ω_k for node k is created by connecting sequentially the mid-edge point to the centroids of the surrounding triangles of the node as shown in Figure 1.

Using the nodal-based smoothing operation, the strains to be used in Equation (23) is assumed to be the *smoothed* strain for node k defined by

$$\widehat{\boldsymbol{\varepsilon}}_k \equiv \widehat{\boldsymbol{\varepsilon}}(\mathbf{x}_k) = \int_{\Omega_k} \boldsymbol{\varepsilon}(\mathbf{x})\, \widehat{\mathbf{W}}(\mathbf{x}-\mathbf{x}_k)\, \mathrm{d}\Omega \tag{25}$$

DOI: 10.1002/nme

where $\widehat{\mathbf{W}} = \lfloor \widehat{W} \ \widehat{W} \ \widehat{W} \rfloor$ is a diagonal matrix of smoothing function $\widehat{W}$. For simplicity, the smoothing function is taken as

$$\widehat{W}(\mathbf{x}-\mathbf{x}_k) = \begin{cases} 1/A_k, & \mathbf{x} \in \Omega_k \\ 0, & \mathbf{x} \notin \Omega_k \end{cases} \tag{26}$$

where $A_k = \int_{\Omega_k} \mathrm{d}\Omega$ is the area of smoothing domain for node k.

Substituting Equation (26) into Equation (25) and integrating by parts, the smoothed strain can be calculated using

$$\widehat{\boldsymbol{\varepsilon}}_k = \frac{1}{A_k} \int_{\Omega_k} \boldsymbol{\varepsilon}(\mathbf{x}) \, \mathrm{d}\Omega = \frac{1}{A_k} \int_{\Gamma_k} \mathbf{L}_n \mathbf{u}(\mathbf{x}) \, \mathrm{d}\Gamma = \widehat{\boldsymbol{\varepsilon}}_k(\mathbf{u}) \tag{27}$$

where Γ_k is the boundary of the smoothing domain for node k, and $\mathbf{L}_n$ is the matrix of the outward normal vector on Γ_k. Equation (27) states the fact that the assumed strain $\widehat{\boldsymbol{\varepsilon}}_k$ is a function of the assumed displacement $\mathbf{u}$.

Substituting Equation (9) into Equation (27), the smoothed strain can be expressed in the following matrix form of nodal displacements:

$$\widehat{\boldsymbol{\varepsilon}}_k = \sum_{i \in N_{\mathrm{infl}}} \widehat{\mathbf{B}}_i(\mathbf{x}_k) \mathbf{d}_i \tag{28}$$

where N_{infl} is the number of nodes in the influence domain of node k (including node k). When linear shape functions are used, it is the number of nodes that is directly connected to node k in the triangular mesh (see Figure 1). In Equation (28), the $\widehat{\mathbf{B}}_i(\mathbf{x}_k)$ is termed as the *smoothed* strain matrix that is calculated using

$$\widehat{\mathbf{B}}_i(\mathbf{x}_k) = \begin{bmatrix} \widehat{b}_{ix}(\mathbf{x}_k) & 0 \\ 0 & \widehat{b}_{iy}(\mathbf{x}_k) \\ \widehat{b}_{iy}(\mathbf{x}_k) & \widehat{b}_{ix}(\mathbf{x}_k) \end{bmatrix} \tag{29}$$

Using the Gauss integration along each segment of boundary Γ_k, we have

$$\widehat{b}_{il} = \frac{1}{A_k} \sum_{m=1}^{N_{\mathrm{s}}} \left[\sum_{n=1}^{N_{\mathrm{g}}} w_n \varphi_i(\mathbf{x}_{mn}) n_l(\mathbf{x}_m) \right] \quad (l = x, y) \tag{30}$$

where N_{s} is the number of segments of the boundary Γ_k, N_{g} is the number of Gauss points used in each segment, w_n is the corresponding weight number of Gauss integration scheme, and n_l is the unit outward normal corresponding to each segment on the smoothing domain boundary. In the LC-PIM using linear shape functions, $n_{\mathrm{g}} = 1$ is used. The entries in sub-matrices of the stiffness matrix $\widehat{\mathbf{K}}$ in Equation (24) are then expressed as

$$\widehat{\mathbf{K}}_{ij} = \sum_{k=1}^{N} \widehat{\mathbf{K}}_{ij(k)} \tag{31}$$

DOI: 10.1002/nme

where the summation means an assembly process as we practice in the FEM, and $\widehat{\mathbf{K}}_{ij(k)}$ is the stiffness matrix associated with node k that is computed using

$$\widehat{\mathbf{K}}_{ij(k)} = \int_{\Omega_k} \widehat{\mathbf{B}}_i^{\mathrm{T}} \mathbf{D} \widehat{\mathbf{B}}_j \, \mathrm{d}\Omega = \widehat{\mathbf{B}}_i^{\mathrm{T}} \mathbf{D} \widehat{\mathbf{B}}_j A_k \tag{32}$$

The entries (in sub-vectors of nodal forces) of the force vector $\widehat{\mathbf{f}}$ in Equation (24) can be simply expressed as

$$\widehat{\mathbf{f}}_i = \sum_{k \in N_{\mathrm{infl}}} \widehat{\mathbf{f}}_{i(k)} \tag{33}$$

The above integration is also performed by a summation of integrals over smoothing domains; hence, $\widehat{\mathbf{f}}_i$ is an assembly of nodal force vectors at the surrounding nodes of node k:

$$\widehat{\mathbf{f}}_{i(k)} = \int_{\Gamma_{t(k)}} \mathbf{\Phi}_i \hat{\mathbf{t}} \, \mathrm{d}\Gamma + \int_{\Omega_{(k)}} \mathbf{\Phi}_i \mathbf{b} \, \mathrm{d}\Omega \tag{34}$$

Note again that the force vector obtained in LC-PIM is the same as that in the FEM, if the same order of shape functions is used. Therefore, it is shown again that there is no difference between $\tilde{\mathbf{f}}$ and $\widehat{\mathbf{f}}$.

4.4. Comparison between FEM and LC-PIM

We now compare the FEM with the LC-PIM.

Remark 4
When FEM and LC-PIM use the same triangular mesh, we have the same set of nodes for nodal displacements and the same size in the discrete system equations and the number of unknowns. The interpolation of displacements in both FEM and LC-PIM is essentially the same. The stiffness matrices have the same sparsity and bandwidth, if the same numbering system for the nodes is used. The stiffness matrices obtained using both FEM and LC-PIM are symmetric-positive definite (SPD), if sufficient constraints are applied to eliminate the rigid body movement. The displacement field in both FEM and LC-PIM is compatible in the global problem domain. Note that when higher-order interpolation schemes are used, FEM and LC-PIM will depart: FEM uses element-based interpolation, but LC-PIM has overlapping in the use of nodes for interpolation.

Remark 5
All the shape functions used in FEM and LC-PIM have the property of the Delta function, which allows straightforward imposition of essential boundary conditions.

Remark 6
The integration in FEM is element based, but the integration in LC-PIM is nodal smoothing domain based.

Remark 7
Both FEM and LC-PIM can reproduce linear displacement field exactly and hence pass the standard patch test (to machine accuracy), if shape functions of at least first order are used. This allows both FEM and LC-PIM converge to the exact solution of any higher-order field.

DOI: 10.1002/nme

Remark 8
The FEM is capable of reproducing any higher-order field, as long as the field lives in the space of the FEM shape functions; LC-PIM can approximate only the high-order field (when Equation (27) is used), even if high-order shape functions are used. In FEM the strains in the element are obtained using Equations (4) and (9); hence, it is a fully compatible mode. In the LC-PIM, however, the strains in the smoothing cells are obtained using Equation (28), and hence will not be compatible within the smoothing cells, in terms of satisfying the displacement–strain relationships.

Remark 9
The FEM solution does not in general satisfy the equilibrium conditions locally (either at any point in the elements or element-wise). The LC-PIM solution, on the other hand, satisfies the equilibrium equations (free of body force) at any point within the smoothing domain, for each of the smoothing domains, and hence at any point in the entire problem domain. However, on the interfaces of the smoothing domains, only the displacement compatibility is ensured. Therefore, the LC-PIM behaves very much like an *equilibrium model*, but not exactly like an equilibrium model. It is a *quasi-equilibrium* model that combines equilibrium model and compatible model.

Remark 10
FEM model using triangular elements behaves very 'stiff', and the stress result is in general not very accurate. The LC-PIM model using exactly the same triangular mesh behaves much softer, and the stress result is in general more accurate.

Remark 11
In terms of convergence rate, for the same problem with the same mesh, the LC-PIM obtains similar values of convergence rate in displacement norm. The convergence rate in energy norm of the LC-PIM with linear elements is, theoretically, between 1.0 and 2.0, which is higher than that of the FEM model with compatible linear elements.

Remark 12
In terms of computational efficiency, for the same problem of the same mesh, the CPU time required by FEM and LC-PIM is in the same level. For a solution of same accuracy in stress, the LC-PIM is more efficient.

Remark 13
For the elasticity problems with homogeneous essential boundary conditions, the displacement-based fully compatible FEM model provides the lower bound for the solution (in energy norm), and the LC-PIM provides the upper bound of the solution, which will be discussed intensively in the following sections.

5. VARIATIONAL PRINCIPLE FOR LC-PIM

5.1. Weak form for LC-PIM

In this section, we discuss in detail about the weak form for the LC-PIM. We first allow two independent field variables: strain field and the displacement field. In this case, we shall have the

DOI: 10.1002/nme

Hellinger–Reissner's two-field variational principle (see, e.g. [19]):

$$J(\mathbf{u},\boldsymbol{\varepsilon}) = -\int_\Omega \frac{1}{2}\boldsymbol{\varepsilon}^{\mathrm{T}}\mathbf{D}\boldsymbol{\varepsilon}\,\mathrm{d}\Omega - \int_\Omega (\mathbf{L}_d^{\mathrm{T}}\boldsymbol{\sigma}+\mathbf{b})^{\mathrm{T}}\mathbf{u}\,\mathrm{d}\Omega$$

$$+\int_{\Gamma_u}\mathbf{t}^{\mathrm{T}}\hat{\mathbf{u}}\,\mathrm{d}\Gamma - \int_{\Gamma_t}(\hat{\mathbf{t}}-\mathbf{t})^{\mathrm{T}}\mathbf{u}\,\mathrm{d}\Gamma \tag{35}$$

where $\boldsymbol{\varepsilon}$ is the assumed strain vector that is independent of $\mathbf{u}$, the stresses $\boldsymbol{\sigma}$ are dependent on the strains $\boldsymbol{\varepsilon}$ through the stress–strain relationship $\boldsymbol{\sigma}=\mathbf{D}\boldsymbol{\varepsilon}$, and $\mathbf{t}$ is the traction on the boundary that is dependent on the stress $\boldsymbol{\sigma}$ in the form of

$$\mathbf{L}_n^{\mathrm{T}}\boldsymbol{\sigma}=\mathbf{t} \tag{36}$$

Using Green's divergence theorem, the second term in the right-hand side of Equation (35) can be further expressed as

$$\int_\Omega (\mathbf{L}_d^{\mathrm{T}}\boldsymbol{\sigma}+\mathbf{b})^{\mathrm{T}}\mathbf{u}\,\mathrm{d}\Omega = \int_\Gamma \mathbf{L}_n^{\mathrm{T}}\boldsymbol{\sigma}\mathbf{u}\,\mathrm{d}\Gamma - \int_\Omega \boldsymbol{\sigma}^{\mathrm{T}}(\mathbf{L}_d\mathbf{u})\,\mathrm{d}\Omega + \int_\Omega \mathbf{b}^{\mathrm{T}}\mathbf{u}\,\mathrm{d}\Omega \tag{37}$$

Substituting Equation (37) into Equation (35) gives

$$J(\mathbf{u},\boldsymbol{\varepsilon}) = -\int_\Omega \frac{1}{2}\boldsymbol{\varepsilon}^{\mathrm{T}}\mathbf{D}\boldsymbol{\varepsilon}\,\mathrm{d}\Omega - \int_\Gamma \mathbf{L}_n^{\mathrm{T}}\boldsymbol{\sigma}\mathbf{u}\,\mathrm{d}\Gamma + \int_\Omega \boldsymbol{\sigma}^{\mathrm{T}}(\mathbf{L}_d\mathbf{u})\,\mathrm{d}\Omega$$

$$-\int_\Omega \mathbf{b}^{\mathrm{T}}\mathbf{u}\,\mathrm{d}\Omega + \int_{\Gamma_u}\mathbf{t}^{\mathrm{T}}\hat{\mathbf{u}}\,\mathrm{d}\Gamma - \int_{\Gamma_t}(\hat{\mathbf{t}}-\mathbf{t})^{\mathrm{T}}\mathbf{u}\,\mathrm{d}\Gamma \tag{38}$$

We now split the second term of the integration over the entire boundary to two integrations over the displacement boundary Γ_u and over the stress boundary Γ_t, and then rearranging these terms in Equation (38) gives

$$J(\mathbf{u},\boldsymbol{\varepsilon}) = -\int_\Omega \frac{1}{2}\boldsymbol{\varepsilon}^{\mathrm{T}}\mathbf{D}\boldsymbol{\varepsilon}\,\mathrm{d}\Omega + \int_\Omega \boldsymbol{\sigma}^{\mathrm{T}}(\mathbf{L}_d\mathbf{u})\,\mathrm{d}\Omega - \int_\Omega \mathbf{b}^{\mathrm{T}}\mathbf{u}\,\mathrm{d}\Omega - \int_{\Gamma_t}\hat{\mathbf{t}}^{\mathrm{T}}\mathbf{u}\,\mathrm{d}\Gamma$$

$$-\int_{\Gamma_u}(\mathbf{L}_n^{\mathrm{T}}\boldsymbol{\sigma}-\mathbf{t}^{\mathrm{T}})\hat{\mathbf{u}}\,\mathrm{d}\Gamma - \int_{\Gamma_t}(\mathbf{L}_n^{\mathrm{T}}\boldsymbol{\sigma}-\mathbf{t}^{\mathrm{T}})\mathbf{u}\,\mathrm{d}\Gamma \tag{39}$$

Using now Equation (36) and substituting $\boldsymbol{\sigma}=\mathbf{D}\boldsymbol{\varepsilon}$, we arrived at

$$J(\mathbf{u},\boldsymbol{\varepsilon}) = -\int_\Omega \frac{1}{2}\boldsymbol{\varepsilon}^{\mathrm{T}}\mathbf{D}\boldsymbol{\varepsilon}\,\mathrm{d}\Omega + \left(-\int_\Omega \mathbf{b}^{\mathrm{T}}\mathbf{u}\,\mathrm{d}\Omega - \int_{\Gamma_t}\hat{\mathbf{t}}^{\mathrm{T}}\mathbf{u}\,\mathrm{d}\Gamma\right) + \int_\Omega (\boldsymbol{\varepsilon}^{\mathrm{T}}\mathbf{D})(\mathbf{L}_d\mathbf{u})\,\mathrm{d}\Omega \tag{40}$$

DOI: 10.1002/nme

Using Equation (27) for any assumed displacement field $\mathbf{u}$, we have the functional of single displacement variable in the form:

$$J(\mathbf{u}) = \underbrace{-\int_\Omega \frac{1}{2}(\widehat{\boldsymbol{\varepsilon}}(\mathbf{u}))^{\mathrm{T}}\mathbf{D}(\widehat{\boldsymbol{\varepsilon}}(\mathbf{u}))\,\mathrm{d}\Omega}_{\widehat{U}(\mathbf{u})} + \underbrace{\left(-\int_\Omega \mathbf{b}^{\mathrm{T}}\mathbf{u}\,\mathrm{d}\Omega - \int_{\Gamma_t}\hat{\mathbf{t}}^{\mathrm{T}}\mathbf{u}\,\mathrm{d}\Gamma\right)}_{W(\mathbf{u})} + \underbrace{\int_\Omega (\widehat{\boldsymbol{\varepsilon}}^{\mathrm{T}}\mathbf{D})\underbrace{(\mathbf{L}_d\mathbf{u})}_{\boldsymbol{\varepsilon}(\mathbf{u})}\,\mathrm{d}\Omega}_{V_{\widehat{\boldsymbol{\varepsilon}}}(\mathbf{u})}$$

$$= -\widehat{U}(\mathbf{u}) + W(\mathbf{u}) + V_{\widehat{\boldsymbol{\varepsilon}}}(\mathbf{u}) \tag{41}$$

where $\widehat{U}(\mathbf{u})$ is the strain energy potential with smoothed strains, $W(\mathbf{u})$ is the work potential of external force, and $V_{\widehat{\boldsymbol{\varepsilon}}}(\mathbf{u})$ is the strain energy potential of the smoothed strains on the assumed displacement field. Let us now examine in detail $V_{\widehat{\boldsymbol{\varepsilon}}}(\mathbf{u})$ in the LC-PIM setting, through which we prove the following remark.

Theorem 1
The LC-PIM is variationally consistent, and the generalized Galerkin weak from Equation (23) is the weak form for LC-PIM.

Proof
In the process of the nodal integration used in LC-PIM, the problem domain Ω is divided into smoothing domains $\Omega = \Omega_1 \cup \Omega_2 \cup \cdots \cup \Omega_N$ each of which contains a node. The smoothing domain Ω_k for the kth node is created by connecting sequentially the mid-edge point to the centroids of the surrounding triangles of the node as shown in Figure 1. Note that due to the smoothing operation, the assumed strains $\widehat{\boldsymbol{\varepsilon}}_k$ are constants in Ω_k and the corresponding stresses $\widehat{\boldsymbol{\sigma}}_k = \mathbf{D}\widehat{\boldsymbol{\varepsilon}}_k$ are thus also constant in ω_k. Therefore, $\boldsymbol{\sigma}$ is bounded and continuous in each of the smoothing domain. Owing to the fact that the shape functions used are linear functions, the strain $\boldsymbol{\varepsilon}$ is also a continuous function in each of the smoothing domain. We then have

$$V_{\widehat{\boldsymbol{\varepsilon}}}(\mathbf{u}) = \int_\Omega \widehat{\boldsymbol{\varepsilon}}^{\mathrm{T}}\mathbf{D}\boldsymbol{\varepsilon}\,\mathrm{d}\Omega = \int_\Omega \widehat{\boldsymbol{\varepsilon}}^{\mathrm{T}}\mathbf{D}(\mathbf{L}_d\mathbf{u})\,\mathrm{d}\Omega = \sum_{k=1}^{N}\int_{\Omega_k}\widehat{\boldsymbol{\varepsilon}}_k^{\mathrm{T}}\mathbf{D}(\mathbf{L}_d\mathbf{u})\,\mathrm{d}\Omega \tag{42}$$

Using Green's divergence theorem for each smoothing domain Ω_k and the fact that $\mathbf{L}_d^{\mathrm{T}}(\widehat{\boldsymbol{\varepsilon}}_k^{\mathrm{T}}\mathbf{D})$ vanishes in Ω_k, we obtain

$$V_{\widehat{\boldsymbol{\varepsilon}}}(\mathbf{u}) = \sum_{k=1}^{N}\left[\int_{\Gamma_k}(\widehat{\boldsymbol{\varepsilon}}_k^{\mathrm{T}}\mathbf{D})(\mathbf{L}_n\mathbf{u})\,\mathrm{d}\Gamma - \int_{\Omega_k}\underbrace{(\mathbf{L}_d^{\mathrm{T}}(\widehat{\boldsymbol{\varepsilon}}_k^{\mathrm{T}}\mathbf{D}))}_{=0,\text{in }\Omega_k^{\mathrm{T}}\mathbf{u}}\,\mathrm{d}\Omega\right]$$

$$= \sum_{k=1}^{N}\int_{\Gamma_k}\widehat{\boldsymbol{\varepsilon}}_k^{\mathrm{T}}\mathbf{D}(\mathbf{L}_n\mathbf{u})\,\mathrm{d}\Gamma \tag{43}$$

DOI: 10.1002/nme

Again since $\widehat{\boldsymbol{\varepsilon}}_k$ is constant in Ω_k, we arrived at

$$V_{\widehat{\boldsymbol{\varepsilon}}}(\mathbf{u}) = \sum_{k=1}^{N} (\widehat{\boldsymbol{\varepsilon}}_k^{\mathrm{T}}\mathbf{D}) \underbrace{\int_{\Gamma_k} (\mathbf{L}_n\mathbf{u})\,\mathrm{d}\Gamma}_{\widehat{\boldsymbol{\varepsilon}}_k A_k} = \sum_{k=1}^{N} \widehat{\boldsymbol{\varepsilon}}_k^{\mathrm{T}}\mathbf{D}\widehat{\boldsymbol{\varepsilon}}_k A_k = \int_{\Omega} \widehat{\boldsymbol{\varepsilon}}^{\mathrm{T}}\mathbf{D}\,\widehat{\boldsymbol{\varepsilon}}\,\mathrm{d}\Omega = 2\,\widehat{U}(\mathbf{u}) \tag{44}$$

In deriving the above equation, we used Equation (27). Equation (44) means that the LC-PIM satisfies the orthogonal conditions [20]:

$$\int_{\Omega} \widehat{\boldsymbol{\varepsilon}}^{\mathrm{T}}\mathbf{D}\boldsymbol{\varepsilon}\,\mathrm{d}\Omega = \int_{\Omega} \widehat{\boldsymbol{\varepsilon}}^{\mathrm{T}}\mathbf{D}\,\widehat{\boldsymbol{\varepsilon}}\,\mathrm{d}\Omega \tag{45}$$

which implies that LC-PIM is *variationally consistent*. □

Substituting the above equation into Equation (41), we have the following energy functional for the LC-PIM:

$$J(\mathbf{u}) = \int_{\Omega} \frac{1}{2}(\widehat{\boldsymbol{\varepsilon}}(\mathbf{u}))^{\mathrm{T}}\mathbf{D}(\widehat{\boldsymbol{\varepsilon}}(\mathbf{u}))\,\mathrm{d}\Omega - \int_{\Omega} \mathbf{b}^{\mathrm{T}}\mathbf{u}\,\mathrm{d}\Omega - \int_{\Gamma_t} \hat{\mathbf{t}}^{\mathrm{T}}\mathbf{u}\,\mathrm{d}\Gamma \tag{46}$$

For any assumed displacement, Equation (46) is a mixed variational principle of the assumed strain method [20], and the corresponding weak form is Equation (23).

Note that the difference between the *standard* Galerkin weak form and the *generalized* Galerkin weak form is that in the standard Galerkin weak form we have to use compatible strains $\boldsymbol{\varepsilon} = \mathbf{L}_d\mathbf{u}$, but in the generalized Galerkin weak form we use an assumed strain $\widehat{\boldsymbol{\varepsilon}}$, which is, in the case of LC-PIM, the smoothed strain given by Equation (28). In general, an assumed strain does not necessarily satisfy the orthogonal condition Equation (45), and the formulation based on the generalized Galerkin weak form will not be variationally consistent. A variationally inconsistent formulation can work well, if it is energy consistent such as in the smoothed FEM or SFEM proposed by Liu *et al.* [21, 22], where a detailed proof for the energy consistence is provided. On the other hand, a variationally consistent formulation does not in general guarantee a stable solution. A typical example is the SFEM, with SC = 1 we can have hourglass instability for some problems [21, 22]. The reason is that due to the use of an assumed strain instead of the compatible strain, the formulation becomes incompatible. Hence, it is well possible that the resultant stiffness matrix (still symmetric) can have intrinsic zero eigenvalues even if the problem is wellposed (physically sufficient support is imposed).

It is well known in FEM [16] that if the number of independent relations provided by all integration points must be no less than the number of unknowns, the stiffness matrix $\mathbf{K}$ must be singular or contain zero eigenvalue. This concept has also been applied to analyze mesh-free methods [9]. Considering now the present LC-PIM for 2D problems, there are three independent strain relations at each node and the total number of independent equations generated in LC-PIM will be $3N$, where N is the total number of field nodes in the whole problem domain. The number of unknown variables should be $2N - N_f$, where N_f is the number of constrained degrees of freedoms (DOFs). It is obvious that the LC-PIM always satisfy the requirement mentioned above, which concludes that the LC-PIM will not encounter the problem of zero eigenvalues or unstable modes. This is also confirmed by the results of all the numerical examples. The LC-PIM will have no zero-energy modes and always be stable as long as the problem is well posed (physically sufficient support is imposed).

DOI: 10.1002/nme

5.2. Upper bound property of LC-PIM

We have discovered recently a very important property of LC-PIM: for the elasticity problem with homogeneous essential boundary conditions, the solution of the LC-PIM has always been the upper bound of the exact solution in energy norm, which will also be shown in all the examples given in the following section. To understand this property, we need to examine closely the relationship between solutions of an LC-PIM model, a FEM model and the exact model that produces the exact solution.

5.2.1. LC-PIM vs FEM. We first present the following lemma.

Lemma 1
For any given admissible displacement field $\mathbf{u}$, the strain potential $\widehat{U}(\mathbf{u})$ for an LC-PIM model obtained using the smoothed strains is no larger than the strain potential $\tilde{U}(\mathbf{u})$ for a FEM model of compatible displacements:

$$\widehat{U}(\mathbf{u}) \leqslant \tilde{U}(\mathbf{u}) \tag{47}$$

in which

$$\widehat{U}(\mathbf{u}) = \int_\Omega \frac{1}{2} \widehat{\boldsymbol{\varepsilon}}^{\mathrm{T}}(\mathbf{u}) \mathbf{D} \widehat{\boldsymbol{\varepsilon}}(\mathbf{u}) \, \mathrm{d}\Omega \tag{48}$$

$$\tilde{U}(\mathbf{u}) = \int_\Omega \frac{1}{2} \tilde{\boldsymbol{\varepsilon}}^{\mathrm{T}}(\mathbf{u}) \mathbf{D} \tilde{\boldsymbol{\varepsilon}}(\mathbf{u}) \, \mathrm{d}\Omega \tag{49}$$

where $\widehat{\boldsymbol{\varepsilon}}$ is the smoothed strain obtained in LC-PIM using Equation (27) and $\tilde{\boldsymbol{\varepsilon}}$ is the strain obtained in FEM.

Proof
We first examine

$$\begin{aligned}
&\int_\Omega \frac{1}{2} (\widehat{\boldsymbol{\varepsilon}} - \tilde{\boldsymbol{\varepsilon}})^{\mathrm{T}} \mathbf{D} (\widehat{\boldsymbol{\varepsilon}} - \tilde{\boldsymbol{\varepsilon}}) \, \mathrm{d}\Omega \\
&= \int_\Omega \frac{1}{2} \widehat{\boldsymbol{\varepsilon}}^{\mathrm{T}} \mathbf{D} \widehat{\boldsymbol{\varepsilon}} \, \mathrm{d}\Omega - \int_\Omega \frac{1}{2} \widehat{\boldsymbol{\varepsilon}}^{\mathrm{T}} \mathbf{D} \tilde{\boldsymbol{\varepsilon}} \, \mathrm{d}\Omega - \int_\Omega \frac{1}{2} \tilde{\boldsymbol{\varepsilon}}^{\mathrm{T}} \mathbf{D} \widehat{\boldsymbol{\varepsilon}} \, \mathrm{d}\Omega + \int_\Omega \frac{1}{2} \tilde{\boldsymbol{\varepsilon}}^{\mathrm{T}} \mathbf{D} \tilde{\boldsymbol{\varepsilon}} \, \mathrm{d}\Omega \\
&= \int_\Omega \frac{1}{2} \widehat{\boldsymbol{\varepsilon}}^{\mathrm{T}} \mathbf{D} \widehat{\boldsymbol{\varepsilon}} \, \mathrm{d}\Omega - \int_\Omega \widehat{\boldsymbol{\varepsilon}}^{\mathrm{T}} \mathbf{D} \tilde{\boldsymbol{\varepsilon}} \, \mathrm{d}\Omega + \int_\Omega \frac{1}{2} \tilde{\boldsymbol{\varepsilon}}^{\mathrm{T}} \mathbf{D} \tilde{\boldsymbol{\varepsilon}} \, \mathrm{d}\Omega
\end{aligned} \tag{50}$$

Using the orthogonal condition that Equation (45) holds for any $\boldsymbol{\varepsilon}$ and the fact that $\tilde{\boldsymbol{\varepsilon}}$ is a special case of $\boldsymbol{\varepsilon}$ and $\mathbf{D}$ is SPD, we have

$$\underbrace{\int_\Omega \frac{1}{2} (\widehat{\boldsymbol{\varepsilon}} - \tilde{\boldsymbol{\varepsilon}})^{\mathrm{T}} \mathbf{D} (\widehat{\boldsymbol{\varepsilon}} - \tilde{\boldsymbol{\varepsilon}}) \, \mathrm{d}\Omega}_{\geqslant 0} = \int_\Omega \frac{1}{2} \tilde{\boldsymbol{\varepsilon}}^{\mathrm{T}} \mathbf{D} \tilde{\boldsymbol{\varepsilon}} \, \mathrm{d}\Omega - \int_\Omega \frac{1}{2} \widehat{\boldsymbol{\varepsilon}}^{\mathrm{T}} \mathbf{D} \widehat{\boldsymbol{\varepsilon}} \, \mathrm{d}\Omega \geqslant 0 \tag{51}$$

which gives Equation (47). □

DOI: 10.1002/nme

Equation (47) can be expressed in discrete form of arbitrary (but admissible) nodal displacement $\mathbf{d}$ as

$$\underbrace{\tfrac{1}{2}\mathbf{d}^{\mathrm{T}}\widehat{\mathbf{K}}\mathbf{d}}_{\widehat{U}(\mathbf{d})} \leqslant \underbrace{\tfrac{1}{2}\mathbf{d}^{\mathrm{T}}\tilde{\mathbf{K}}\mathbf{d}}_{\tilde{U}(\mathbf{d})} \tag{52}$$

Corollary 1
For any admissible assumed nodal displacement field $\mathbf{d}$, the total potential $\tilde{J}(\mathbf{d})$ for FEM model is no less than that of $\widehat{J}(\mathbf{d})$ for LC-PIM model:

$$\tilde{J}(\mathbf{d}) \geqslant \widehat{J}(\mathbf{d}) \tag{53}$$

where

$$\tilde{J}(\mathbf{d}) = \tfrac{1}{2}\mathbf{d}^{\mathrm{T}}\tilde{\mathbf{K}}\mathbf{d} - \mathbf{d}^{\mathrm{T}}\tilde{\mathbf{f}} \tag{54}$$

$$\widehat{J}(\mathbf{d}) = \tfrac{1}{2}\mathbf{d}^{\mathrm{T}}\widehat{\mathbf{K}}\mathbf{d} - \mathbf{d}^{\mathrm{T}}\widehat{\mathbf{f}} \tag{55}$$

Proof
This is a natural consequence of Lemma 1, based on the fact that $\tilde{\mathbf{f}}$ and $\widehat{\mathbf{f}}$ are the same. □

Theorem 2
When the same mesh is used, the strain energy obtained from the LC-PIM solution is no less than that from the FEM solution based on compatible displacement model:

$$\widehat{U}(\widehat{\mathbf{d}}) \geqslant \tilde{U}(\tilde{\mathbf{d}}) \tag{56}$$

where

$$\widehat{U}(\widehat{\mathbf{d}}) = \tfrac{1}{2}\widehat{\mathbf{d}}^{\mathrm{T}}\widehat{\mathbf{K}}\widehat{\mathbf{d}} \tag{57}$$

$$\tilde{U}(\tilde{\mathbf{d}}) = \tfrac{1}{2}\tilde{\mathbf{d}}^{\mathrm{T}}\tilde{\mathbf{K}}\tilde{\mathbf{d}} \tag{58}$$

The equality is true when LC-PIM and FEM produce the exact solutions or all the nodal-based smoothing covers only on element.

Proof
On the basis of Lemma 1 (see Equation (52)), we obtain for *any* admissible $\mathbf{d}$:

$$\underbrace{\mathbf{d}^{\mathrm{T}}\tilde{\mathbf{K}}d - \mathbf{d}^{\mathrm{T}}\widehat{\mathbf{K}}\mathbf{d}}_{\geqslant 0} = \mathbf{d}^{\mathrm{T}}(\tilde{\mathbf{K}} - \widehat{\mathbf{K}})\mathbf{d} \geqslant 0 \tag{59}$$

Equation (59) implies that matrix $(\tilde{\mathbf{K}} - \widehat{\mathbf{K}})$ is SPD. In mechanics, it implies that $\tilde{\mathbf{K}}$ is 'stiffer' than $\widehat{\mathbf{K}}$. In addition, the solution of FEM can be expressed as

$$\tilde{\mathbf{d}} = \tilde{\mathbf{K}}^{-1}\tilde{\mathbf{f}} \tag{60}$$

DOI: 10.1002/nme

in which $\tilde{J}(\mathbf{d})$ is stationary. The solution of LC-PIM can be expressed as

$$\widehat{\mathbf{d}} = \widehat{\mathbf{K}}^{-1}\tilde{\mathbf{f}} \tag{61}$$

in which $\widehat{J}(\mathbf{d})$ is stationary. Note here that we used the fact that $\widehat{\mathbf{f}} = \tilde{\mathbf{f}}$. At the stationary point, we have for FEM

$$\tilde{J}(\tilde{\mathbf{d}}) = \tfrac{1}{2}\tilde{\mathbf{d}}^{\mathrm{T}}\tilde{\mathbf{K}}\tilde{\mathbf{d}} - \tilde{\mathbf{d}}^{\mathrm{T}}\tilde{\mathbf{f}} = -\underbrace{\tfrac{1}{2}\tilde{\mathbf{d}}^{\mathrm{T}}\tilde{\mathbf{K}}\tilde{\mathbf{d}}}_{\tilde{U}(\tilde{\mathbf{d}})} = -\tfrac{1}{2}\tilde{\mathbf{d}}^{\mathrm{T}}\tilde{\mathbf{f}} = -\underbrace{\tfrac{1}{2}\tilde{\mathbf{f}}^{\mathrm{T}}\tilde{\mathbf{K}}^{-1}\tilde{\mathbf{f}}}_{\tilde{U}(\tilde{\mathbf{d}})} \tag{62}$$

and for LC-PIM

$$\widehat{J}(\widehat{\mathbf{d}}) = \tfrac{1}{2}\widehat{\mathbf{d}}^{\mathrm{T}}\widehat{\mathbf{K}}\widehat{\mathbf{d}} - \widehat{\mathbf{d}}^{\mathrm{T}}\tilde{\mathbf{f}} = -\underbrace{\tfrac{1}{2}\widehat{\mathbf{d}}^{\mathrm{T}}\widehat{\mathbf{K}}\widehat{\mathbf{d}}}_{\widehat{U}(\widehat{\mathbf{d}})} = -\tfrac{1}{2}\widehat{\mathbf{d}}^{\mathrm{T}}\tilde{\mathbf{f}} = -\underbrace{\tfrac{1}{2}\tilde{\mathbf{f}}^{\mathrm{T}}\widehat{\mathbf{K}}^{-1}\tilde{\mathbf{f}}}_{\widehat{U}(\widehat{\mathbf{d}})} \tag{63}$$

The difference between the strain energies of FEM and LC-PIM solution becomes

$$\widehat{U}(\widehat{\mathbf{d}}) - \tilde{U}(\tilde{\mathbf{d}}) = \tfrac{1}{2}\tilde{\mathbf{f}}^{\mathrm{T}}\widehat{\mathbf{K}}^{-1}\tilde{\mathbf{f}} - \tfrac{1}{2}\tilde{\mathbf{f}}^{\mathrm{T}}\tilde{\mathbf{K}}^{-1}\tilde{\mathbf{f}} = \tfrac{1}{2}\tilde{\mathbf{f}}^{\mathrm{T}}\underbrace{(\widehat{\mathbf{K}}^{-1} - \tilde{\mathbf{K}}^{-1})}_{\mathrm{SPD}}\tilde{\mathbf{f}} \geqslant 0 \tag{64}$$

which gives Equation (56). □

In the working of Equation (64), we used the fact that $(\widehat{\mathbf{K}}^{-1} - \tilde{\mathbf{K}}^{-1})$ is SPD. This can be proven based on the facts that $\widehat{\mathbf{K}}$, $\tilde{\mathbf{K}}$, and $(\tilde{\mathbf{K}} - \widehat{\mathbf{K}})$ are all SPD (see Equation (59)).

5.2.2. LC-PIM vs exact model. We have found further in our past numerical examples that not only $\widehat{U}(\widehat{\mathbf{d}}) \geqslant \tilde{U}(\tilde{\mathbf{d}})$ but also $\widehat{U}(\widehat{\mathbf{d}}) \geqslant U(\boldsymbol{\varepsilon}) \geqslant \tilde{U}(\tilde{\mathbf{d}})$ is true except for a few trivial cases, which means the solution of LC-PIM gives the upper bound of the exact solution in energy norm. The fact will be stated in Theorem 3 that follows the following lemma.

Lemma 2
For any (admissible) displacement $\mathbf{u}$, the strain potential $\widehat{U}(\mathbf{u})$ for an LC-PIM model is no larger than that of $U(\mathbf{u})$ for the exact model:

$$\widehat{U}(\mathbf{u}) \leqslant U(\mathbf{u}) \tag{65}$$

where

$$\widehat{U}(\mathbf{u}) = \int_{\Omega} \frac{1}{2}\,\widehat{\boldsymbol{\varepsilon}}^{\mathrm{T}}(\mathbf{u})\mathbf{D}\,\widehat{\boldsymbol{\varepsilon}}(\mathbf{u})\,\mathrm{d}\Omega \tag{66}$$

with the smoothed strain $\widehat{\boldsymbol{\varepsilon}}$ obtained using Equation (28), and

$$U(\mathbf{u}) = \int_{\Omega} \frac{1}{2}\boldsymbol{\varepsilon}^{\mathrm{T}}(\mathbf{u})\mathbf{D}\boldsymbol{\varepsilon}(\mathbf{u})\,\mathrm{d}\Omega \tag{67}$$

with the strain $\boldsymbol{\varepsilon}$ obtained using Equation (4).

DOI: 10.1002/nme

Proof
We examine

$$\begin{aligned}
&\int_\Omega \frac{1}{2}(\widehat{\boldsymbol{\varepsilon}}-\boldsymbol{\varepsilon})^{\mathrm{T}}\mathbf{D}(\widehat{\boldsymbol{\varepsilon}}-\boldsymbol{\varepsilon})\,\mathrm{d}\Omega \\
&\quad=\int_\Omega \frac{1}{2}\,\widehat{\boldsymbol{\varepsilon}}^{\mathrm{T}}\mathbf{D}\,\widehat{\boldsymbol{\varepsilon}}\,\mathrm{d}\Omega-\int_\Omega \frac{1}{2}\,\widehat{\boldsymbol{\varepsilon}}^{\mathrm{T}}\mathbf{D}\boldsymbol{\varepsilon}\,\mathrm{d}\Omega-\int_\Omega \frac{1}{2}\boldsymbol{\varepsilon}^{\mathrm{T}}\mathbf{D}\,\widehat{\boldsymbol{\varepsilon}}\,\mathrm{d}\Omega+\int_\Omega \frac{1}{2}\boldsymbol{\varepsilon}^{\mathrm{T}}\mathbf{D}\boldsymbol{\varepsilon}\,\mathrm{d}\Omega \\
&\quad=\int_\Omega \frac{1}{2}\,\widehat{\boldsymbol{\varepsilon}}^{\mathrm{T}}\mathbf{D}\,\widehat{\varepsilon}\,\mathrm{d}\Omega-\int_\Omega \widehat{\boldsymbol{\varepsilon}}^{\mathrm{T}}\mathbf{D}\boldsymbol{\varepsilon}\,\mathrm{d}\Omega+\int_\Omega \frac{1}{2}\boldsymbol{\varepsilon}^{\mathrm{T}}\mathbf{D}\boldsymbol{\varepsilon}\,\mathrm{d}\Omega
\end{aligned} \tag{68}$$

Using the orthogonal condition Equation (45) and the fact that $\mathbf{D}$ is SPD, we have

$$\underbrace{\int_\Omega \frac{1}{2}(\widehat{\boldsymbol{\varepsilon}}-\boldsymbol{\varepsilon})^{\mathrm{T}}\mathbf{D}(\widehat{\boldsymbol{\varepsilon}}-\boldsymbol{\varepsilon})\,\mathrm{d}\Omega}_{\geqslant 0}=\int_\Omega \frac{1}{2}\boldsymbol{\varepsilon}^{\mathrm{T}}\mathbf{D}\boldsymbol{\varepsilon}\,\mathrm{d}\Omega-\int_\Omega \frac{1}{2}\,\widehat{\boldsymbol{\varepsilon}}^{\mathrm{T}}\mathbf{D}\,\widehat{\varepsilon}\,\mathrm{d}\Omega\geqslant 0 \tag{69}$$

which gives Equation (65). □

Corollary 2
For any assumed admissible nodal displacement field $\mathbf{d}$, the total potential $J(\mathbf{d})$ for the exact model is no less than that of $\widehat{J}(\mathbf{d})$ for LC-PIM model:

$$J(\mathbf{d})\geqslant \widehat{J}(\mathbf{d}) \tag{70}$$

where

$$\begin{aligned}
J(\mathbf{d}) &= \tfrac{1}{2}\mathbf{d}^{\mathrm{T}}\mathbf{K}\mathbf{d}-\mathbf{d}^{\mathrm{T}}\mathbf{f} \\
\widehat{J}(\mathbf{d}) &= \tfrac{1}{2}\mathbf{d}^{\mathrm{T}}\widehat{\mathbf{K}}\mathbf{d}-\mathbf{d}^{\mathrm{T}}\widehat{\mathbf{f}}
\end{aligned} \tag{71}$$

Proof
This is natural consequence of Lemma 2, based on the fact that $\mathbf{f}$ and $\widehat{\mathbf{f}}$ are the same. □

Theorem 3
The strain energy obtained from the LC-PIM solution has the following relationship with the exact strain energy:

$$\widehat{U}(\widehat{\mathbf{d}})\geqslant U(\mathbf{d}_0) \tag{72}$$

where $\widehat{\mathbf{d}}$ is the solution of an LC-PIM model, which is obtained using shape functions constructed using bases containing the exact solution and used in Equation (9), and $\mathbf{d}_0$ is the exact nodal displacement sampled using the exact displacement field $\mathbf{u}_0$.

DOI: 10.1002/nme

Proof
Consider a problem with the exact solution of $\mathbf{u}_0$. Let $\mathbf{d}_0$ be the corresponding solution at the nodes of the mesh used in the LC-PIM model for the same problem. The exact solution $\mathbf{u}_0$ can then always be expressed in the form:

$$\mathbf{u}_0(\mathbf{x}, \mathbf{d}) = \sum_{i \in n_e} \mathbf{\Phi}_{ei}(\mathbf{x}) \mathbf{d}_{0i} \tag{73}$$

where n_e is the set of nodes of the element containing $\mathbf{x}$, $\mathbf{d}_{0i}$ is the vector of nodal displacements of the exact solution, and $\mathbf{\Phi}_{ei}(\mathbf{x})$ is the matrix of the shape functions that are constructed using bases containing the exact solution in the form of Equation (10) that returns $\mathbf{u}_0$ for the given $\mathbf{d}_{0i}$ within the element. We now consider an arbitrary displacement field defined by

$$\mathbf{u}(\mathbf{x}, \mathbf{d}) = \sum_{i \in n_e} \mathbf{\Phi}_{ei}(\mathbf{x}) \mathbf{d}_i \tag{74}$$

where $\mathbf{d}_i$ is the vector of arbitrary nodal displacements. This means that we have a *special* FEM model that uses the exact shape function, which should produce the exact solution of nodal displacement (Remark 3). Following the arguments in proving Theorem 2, we should have

$$\widehat{U}(\widehat{\mathbf{d}}) - U(\mathbf{d}_0) \geqslant 0 \tag{75}$$

which is Equation (72). □

5.2.3. The battle of softening and stiffening effects. Theorem 3 implies that LC-PIM can provide an upper bound for the exact solution in energy norm, under the condition that $\mathbf{\Phi}_{ei}(\mathbf{x})$ is used. In mechanics, this means that the smoothing operation provides a *softening* effect to the solids or structure, so that the displacement $\widehat{\mathbf{d}}$ obtained by LC-PIM is 'larger' (in $\mathbf{K}$ norm) than that of the exact solution.

In the practice of using LC-PIM for a general problem, however, finding $\mathbf{\Phi}_{ei}(\mathbf{x})$ is not always practical. Therefore, we use the usual PIM shape functions (or, in special cases, the FEM shape functions) instead. The use of any (compatible) shape functions in the place of the exact shape functions will, on the other hand, provide a *stiffening* effect to the model. The battle between the softening and stiffening effects will determine whether an LC-PIM model can in fact provide an upper bound solution to the problem.

The *softening effect* depends on the following situations in an LC-PIM model.

- The number of elements that is connected to a node of a smoothing domain: The more the elements, the more the smoothing effects. As shown in Figure 1, at node k, there are five elements connected, and at the corner node q, however, only two elements are connected. In an extreme case, if the smoothing domain is defined for each element to perform the smoothing operation (Ω_k is further divided into five sub-domains: each for an element), there will not be any softening effect. In this case, the LC-PIM and FEM give naturally the same results, and the LC-PIM will not provide an upper bound, but a lower bound solution.
- The number of nodes being smoothed: In LC-PIM, one does not have to perform the smoothing operation for all the nodes. If the smoothing is selectively performed, the softening effect will propositionally depend on the number of nodes participated in the smoothing operation.
- The number of nodes used in the problem domain or density of the background cells: When a small number of nodes are used, the displacements approximated using the PIM shape

DOI: 10.1002/nme

functions in a smoothing domain deviate far from the exact solution, resulting in a heavy smoothing to the strain field, and hence a strong softening effect. On the other hand, When a large number of nodes are used, the displacements approximated using the PIM shape functions in a smoothing domain are more close to the exact solution, resulting in less smoothing effects, and hence less softening effect. At the extreme of infinitely small elements are used, the smoothing effects will diminish and the LC-PIM solution (also the FEM solution) will approach to the exact solution.

The *stiffening effect* depends on the following situations in an LC-PIM model.

- The order of the PIM shape functions used in the displacement approximation: when high-order PIM shape functions are used, the displacements approximated using the PIM shape functions in a smoothing domain are closer to the exact solution of displacements, which reduces the stiffening effect and *vice versa.*
- The number of nodes used in the problem domain. When a small number of nodes are used, the displacements approximated using the PIM shape functions in a smoothing domain deviate far from the exact solution; the stiffening effect is therefore large, and *vice versa*. At the extreme of infinitely small elements are used, the stiffening effects will diminish and the LC-PIM solution (also the FEM solution) will approach to the exact solution.

Generally, the softening effect provided by the smoothing in an LC-PIM model is more significant than the stiffening effects. This is because the smoothing is a zero-order approximation that is lower than the at least first-order approximation of the displacement resulting in the stiffening effect. Therefore, the LC-PIM always produces an upper bound solution except the following case:

- Only one element is used. In this case, only element participates in smoothing, which should not have any smoothing effects; hence, the solutions of LC-PIM and FEM are the same, and LC-PIM gives a lower bound solution.

In our numerical study, we found that LC-PIM can produce upper bound solutions for all the problems we have studied, except the very special case mentioned above. Intensive numerical studies have been conducted and reported in the following section to confirm the properties of the LC-PIM with a focus on the important upper bound property.

6. NUMERICAL EXAMPLES

To investigate quantitatively the numerical results, the error indicators in displacement and energy norms are defined as follows:

$$e_d = \sqrt{\frac{\sum_{i=1}^{n} (u_i^{\text{exact}} - u_i^{\text{numerical}})^2}{\sum_{i=1}^{n} (u_i^{\text{exact}})^2}} \tag{76}$$

$$e_e = \frac{1}{A}\sqrt{\frac{1}{2}\int_{\Omega} (\boldsymbol{\varepsilon}^{\text{exact}} - \boldsymbol{\varepsilon}^{\text{numerical}})^{\text{T}} \mathbf{D} (\boldsymbol{\varepsilon}^{\text{exact}} - \boldsymbol{\varepsilon}^{\text{numerical}})\, \mathrm{d}\Omega} \tag{77}$$

DOI: 10.1002/nme

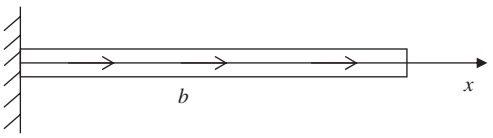

Figure 2. One-dimensional bar subjected to a uniformly distributed body force.

where the superscript exact denotes the exact or analytical solution, numerical denotes the numerical solution obtained using a numerical method including the present LC-PIM, and A is the area of the problem domain.

To demonstrate the upper bound property of LC-PIM numerically, strain energy of the model will be calculated according to the following formula:

$$U = \int_{\Omega} \frac{1}{2} \boldsymbol{\varepsilon}^{\mathrm{T}} \mathbf{D} \boldsymbol{\varepsilon} \, \mathrm{d}\Omega \tag{78}$$

6.1. 1D bar problem

Consider a bar with length L and of uniform cross-sectional area A. As shown in Figure 2, the bar is fixed at the left end and subjected to a uniform body force b. The parameters are taken as $L = 1\,\mathrm{m}$, $A = 1\,\mathrm{m}^2$, $b = 1\,\mathrm{N/m}$, and $E = 1.0\,\mathrm{Pa}$. Governing equation and boundary conditions are as follows:

$$E \frac{\mathrm{d}^2 u}{\mathrm{d}x^2} + 1 = 0 \tag{79}$$

$$\begin{aligned} u(x=0) &= 0 \\ \sigma(x=1) &= 0 \end{aligned} \tag{80}$$

The analytical solution that satisfy the above equations is obtained as

$$u_0(x) = -\frac{1}{2E} x^2 + \frac{1}{E} x \tag{81}$$

The exact strain energy of the problem can be calculated as follows:

$$U(\mathbf{u}_0) = \frac{1}{2} \int_l \boldsymbol{\varepsilon}_0^{\mathrm{T}} E \boldsymbol{\varepsilon}_0 \, \mathrm{d}l = \frac{1}{6E} \tag{82}$$

First, the effect of the dimension of smoothing domain is studied using this simple 1D problem. As shown in Figure 3(a), the problem domain of the bar is presented using three nodes: node 1 located at the left end, node 2 located at the midpoint of the problem domain, and node 3 located at the right end. Cells (1) and (2) are two background cells. Normally, the smoothing length (domain) for node 2 is obtained by connecting the midpoints of cells (1) and (2), which is $l/2$. We now intentionally change the dimension of the smoothing length for node 2 to study its effect on the computed strain energy. As shown in Figure 3(b), the strain energy of LC-PIM model increases with the increase in the smoothing length, which is defined as the ratio of the smoothing length of node 2 to the entire problem domain length l. When the smoothing length reduces to zero (meaning that node 2 contributes nothing to the stiffness), the LC-PIM solution that resulted from

DOI: 10.1002/nme

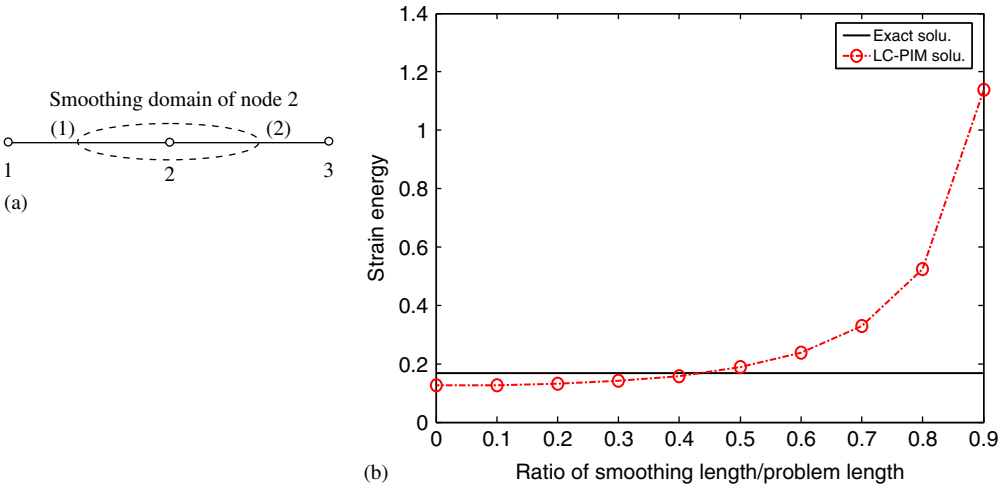

Figure 3. Illustration of the effect of the length of the smoothing domain for 1D problems.

this 3-node model will be the same as that of the FEM solution using one element of 2-nodes, which gives the lower bound solution. When the ratio of the smoothing length increases to about 0.43, the LC-PIM solution of strain energy will be larger than that of the exact solution, providing an upper bound. This finding confirms the discussions given in Section 5.2.3.

Next, six models of different numbers of uniformly distributed nodes are used to study the properties of the solutions of both LC-PIM and FEM. The computed values of strain energy are plotted in Figure 4 against the number of nodes used, together with the exact solution. It can be found that LC-PIM produces same results as FEM when only two nodes are used. In this case, two smoothing domains are used for, respectively, the two field nodes; hence, the smoothing has no effect at all to the problem, and the solution is the same as the FEM giving a lower bound. When the number of nodes is larger than 2, the smoothing takes effect, and the LC-PIM provides an upper bound solution. With the increase in the number of nodes, the FEM solution approaches from below to the exact solution monotonically (see Remark 2); LC-PIM solution, however, approaches from above to the exact solution monotonically, due to the fact that the smoothing effects in the LC-PIM reduce as the displacement filed approaches to the exact solution. These findings confirm again the discussions given in Section 5.2.3. This simple 1D example shows for the first time clearly the very important fact that we now can bound the exact solution from both sides.

6.2. 2D cantilever solid

A 2D cantilever solid with length L and height D is now studied. The solid is subjected to a parabolic traction at the free end as shown in Figure 5. The solid is assumed to have unit thickness, and the following analytical solution based on the plane stress theory is available [23] for our precise examination of the properties of LC-PIM solution:

$$u_x = -\frac{Py}{6EI}\left[(6L-3x)x+(2+\nu)\left(y^2-\frac{D^2}{4}\right)\right] \tag{83}$$

DOI: 10.1002/nme

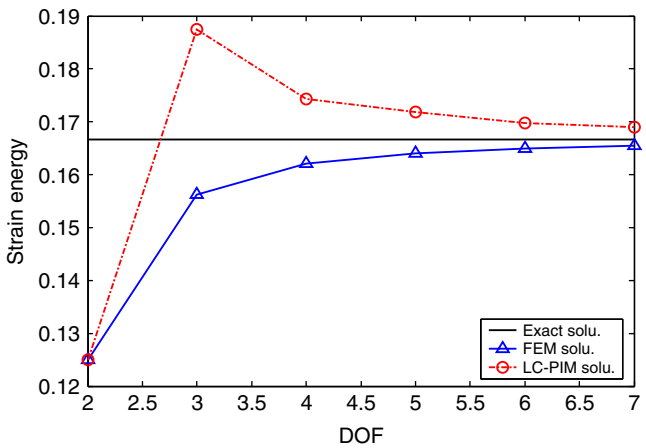

Figure 4. Upper bound solution obtained using the LC-PIM for the 1D bar problem. The lower bound solution is obtained using the FEM using linear elements.

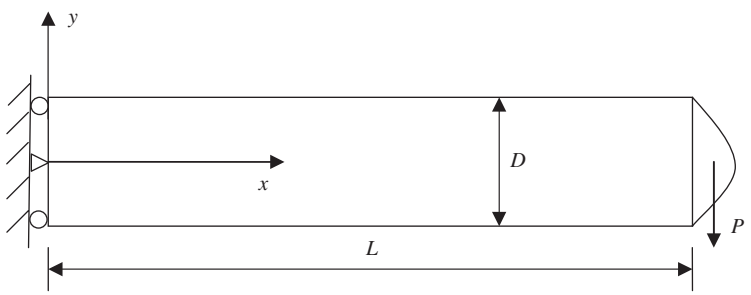

Figure 5. A 2D cantilever solid subjected to a parabolic traction on the right edge.

$$u_y = \frac{P}{6EI}\left[3vy^2(L-x)+(4+5v)\frac{D^2x}{4}+(3L-x)x^2\right] \tag{84}$$

$$\sigma_{xx} = -\frac{P(L-x)y}{I} \tag{85}$$

$$\sigma_{yy} = 0 \tag{86}$$

$$\sigma_{xy} = \frac{P}{2I}\left[\frac{D^2}{4}-y^2\right] \tag{87}$$

where I is the moment of the inertia given as $I = D^3/12$.

Other parameters used in the computation are $E = 3.0\times10^7$ Pa, $v = 0.3$, $L = 50$ m, $D = 10$ m, and $P = -1000$ N.

To study the convergence property of the LC-PIM solution, three models with regularly distributed nodes (105, 369, and 1377 nodes, respectively) have been analyzed. The same problem

DOI: 10.1002/nme

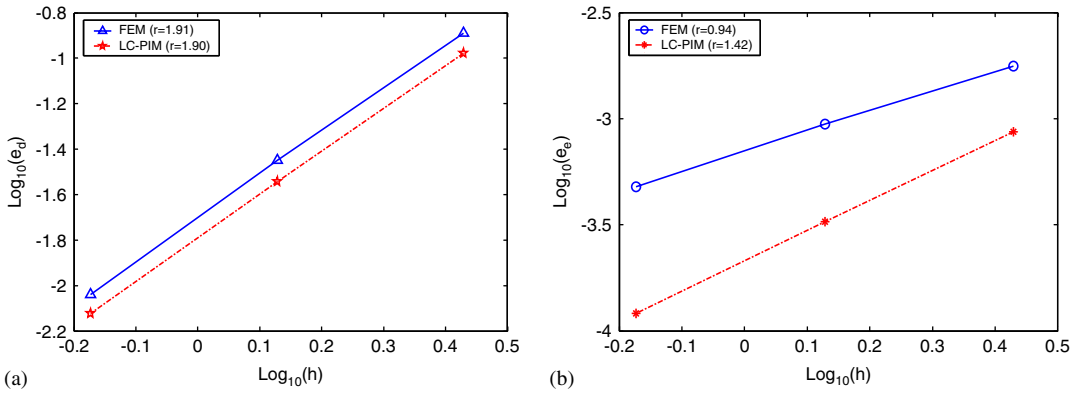

Figure 6. Comparison of convergence rate between the linear FEM and the LC-PIM for the problem of cantilever solid: (a) comparison of convergence rate in displacement norm and (b) comparison of convergence rate in energy norm.

is also analyzed using the linear FEM with the same models. Using Equations (76) and (77), errors in displacement and energy norms are calculated and plotted against the average nodal spacing (h) as shown in Figure 6 . It can be found that the LC-PIM obtains a similar accuracy and convergence rate in displacement compared with the linear FEM. For the results in energy norm, however, solutions of the LC-PIM are more accurate and achieve much higher convergence rate.

It is known that if a fully (both displacements and displacement–strain relationships) compatible model is used, the convergence rate in energy norm should be, theoretically, 1.0 (for linear fields assumed), and if a fully equilibrium model is used, the convergence rate in energy norm should be, theoretically, 2.0. In the LC-PIM, the strain smoothing is performed, which creates an 'equilibrium' state locally inside the smoothing cells. On all the interfaces of the smoothing cells, however, the equilibrium is not ensured and only the compatibility of displacements is ensured. Therefore, the rate of convergence in energy norm should be, theoretically, between 1.0 and 2.0. The actual value will be problem dependent. For this cantilever beam problem, the convergence rate in energy norm for the LC-PIM is 1.42 (shown in Figure 6), which also demonstrated this theory.

Figure 7 shows the convergence status of the strain energies against the increase of DOF for both FEM and LC-PIM. The exact solution of the strain energy is calculated using the analytical solutions of stress components. It can be clearly observed that the strain energy of FEM model is always smaller than the exact solution; on the contrary, the strain energy of LC-PIM model is always larger than the exact solution. The results confirm that for this 2D problem LC-PIM provides upper bound solution. The figure also shows that with the increase in DOF, the strain energy of the FEM model and the LC-PIM model converges to the reference solution from below and above, respectively. This 2D example shows clearly again the very important fact that we now can bound the *exact* solution from both sides.

6.3. Infinite 2D solid with a circular hole

An infinite 2D solid with a central circular hole ($a=1\,\mathrm{m}$) and subjected to a unidirectional tensile ($T_x=10\,\mathrm{N/m}$) is studied. Owing to its two-fold symmetry, one quarter is modeled with $b=5\,\mathrm{m}$ (as shown in Figure 8). Symmetry conditions are imposed on the left and bottom edges, and the

DOI: 10.1002/nme

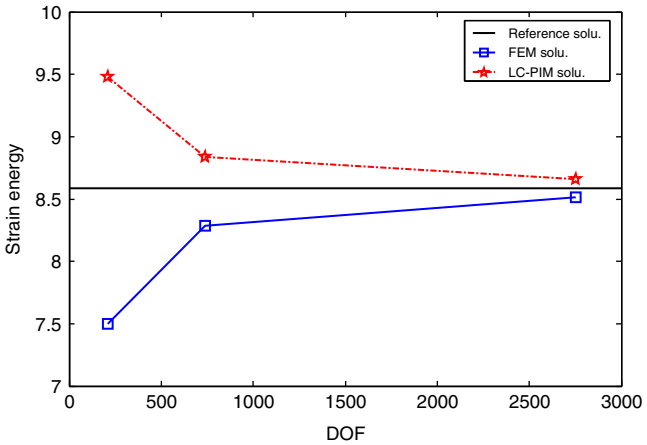

Figure 7. Upper bound solution obtained using the LC-PIM for the problem of cantilever solid. The lower bound solution is obtained using the FEM using linear elements.

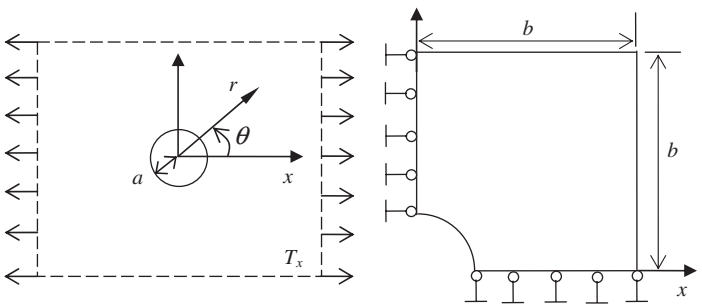

Figure 8. Infinite 2D solid with a circular hole subjected to a tensile force and its quarter model.

inner boundary of the hole is traction free. For this benchmark problem, the analytical solution for the stress is given by [23]

$$\sigma_{xx} = T_x \left\{ 1 - \frac{a^2}{r^2} \left[\frac{3}{2}\cos(2\theta) + \cos(4\theta) \right] + \frac{3a^4}{2r^4}\cos(4\theta) \right\} \tag{88}$$

$$\sigma_{yy} = -T_x \left\{ \frac{a^2}{r^2} \left[\frac{1}{2}\cos(2\theta) - \cos(4\theta) \right] + \frac{3a^4}{2r^4}\cos(4\theta) \right\} \tag{89}$$

$$\sigma_{xy} = -T_x \left\{ \frac{a^2}{r^2} \left[\frac{1}{2}\sin(2\theta) + \sin(4\theta) \right] - \frac{3a^4}{2r^4}\sin(4\theta) \right\} \tag{90}$$

where (r, θ) are the polar coordinates and θ is measured counterclockwise from the positive *x-axis*.

Traction boundary conditions are imposed on the right ($x = 5$ m) and upper ($y = 5$ m) edges based on the analytical solutions in Equations (88)– (90). The displacement components corresponding

DOI: 10.1002/nme

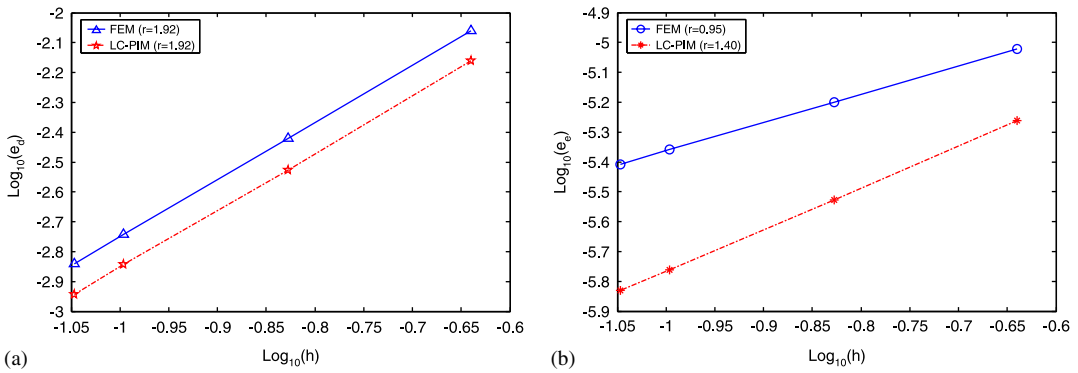

Figure 9. Comparison of convergence rate between the linear FEM and the LC-PIM *via* the infinite solid with a hole: (a) comparison of convergence rate in displacement norm and (b) comparison of convergence rate in energy norm.

to the stress are

$$u_r = \frac{T_x}{4\mu}\left\{r\left[\frac{(\kappa-1)}{2}+\cos(2\theta)\right]+\frac{a^2}{r}\left[1+(1+\kappa)\cos(2\theta)\right]-\frac{a^4}{r^3}\cos(2\theta)\right\} \tag{91}$$

$$u_\theta = \frac{T_x}{4\mu}\left[(1-\kappa)\frac{a^2}{r}-r-\frac{a^4}{r^3}\right]\sin(2\theta) \tag{92}$$

where

$$\mu=\frac{E}{2(1+v)}, \quad \kappa=\begin{cases}3-4v & \text{plane strain}\\ \dfrac{3-v}{1+v} & \text{plane stress}\end{cases} \tag{93}$$

The problem domain is discretized with four models of irregularly distributed nodes (577, 1330, 2850, and 3578 nodes, respectively). The convergence rates in displacement and energy norms are demonstrated in Figure 9 for both the FEM and the LC-PIM. Again, it can be seen that for the displacement results, the LC-PIM and the FEM obtain similar accuracy and achieve an almost-equal convergence rate, but for the stress results in energy norm, the LC-PIM provides better accuracy and achieves much higher convergence rate.

The strain energy for each model is calculated for both FEM and LC-PIM. As shown in Figure 10, the strain energy of the FEM model is always smaller than the exact solution and converges from below with the increase in DOF. On the contrary, the strain energy of the LC-PIM model is always larger than the exact solution and converges from above. The results confirm again for this 2D problem that LC-PIM provides upper bound solution.

6.4. 2D half space

A 2D half space subjected to a uniform pressure on the upper surface within a finite range ($-a \leqslant x \leqslant a$) is studied (as shown in Figure 11). Plane strain condition is considered and the

DOI: 10.1002/nme

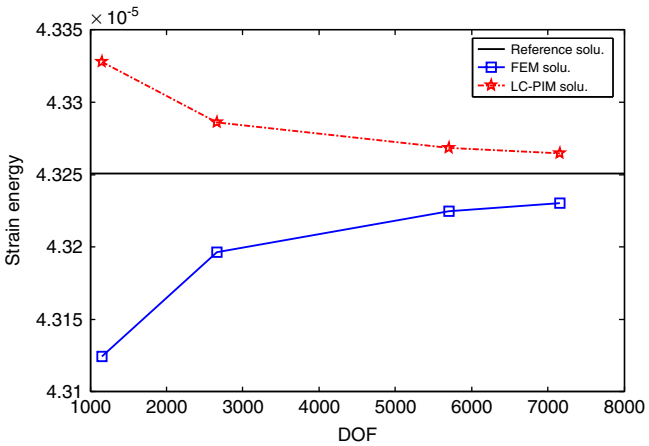

Figure 10. Upper bound solution obtained using the LC-PIM for the problem of infinite solid with a hole. The lower bound solution is obtained using the FEM using linear elements.

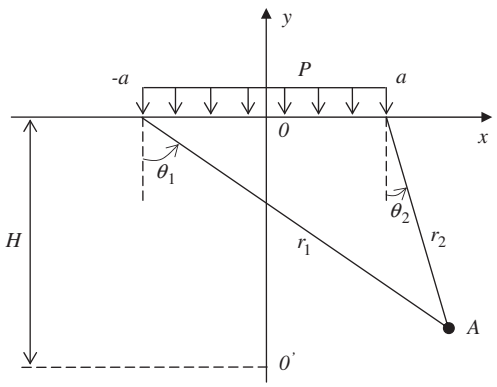

Figure 11. Semi-infinite 2D solid subjected to a uniform pressure on the surface.

analytical stresses are given by [23]

$$\sigma_{xx} = \frac{p}{2\pi}[2(\theta_1 - \theta_2) - \sin 2\theta_1 + \sin 2\theta_2] \tag{94}$$

$$\sigma_{yy} = \frac{p}{2\pi}[2(\theta_1 - \theta_2) + \sin 2\theta_1 - \sin 2\theta_2] \tag{95}$$

$$\sigma_{xy} = \frac{p}{2\pi}(\cos 2\theta_1 - \cos 2\theta_2) \tag{96}$$

DOI: 10.1002/nme

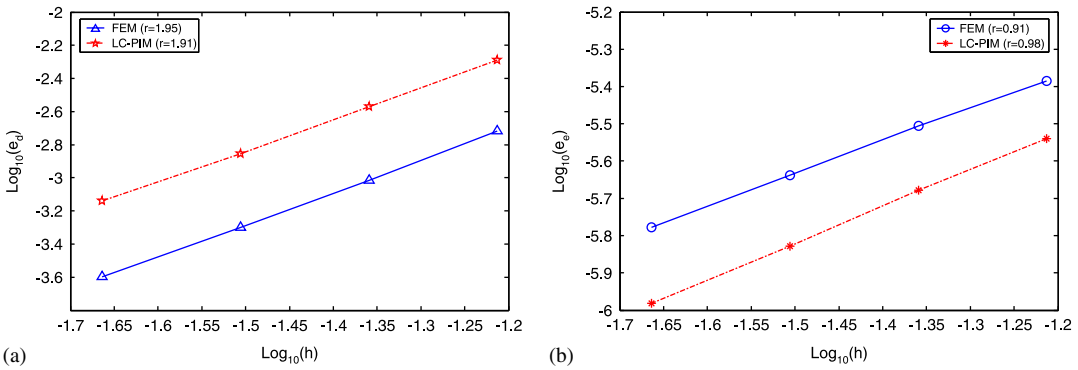

Figure 12. Comparison of convergence rate between the linear FEM and the LC-PIM *via* the problem of semi-infinite plane: (a) comparison of convergence rate in displacement norm and (b) comparison of convergence rate in energy norm.

The directions of θ_1 and θ_2 are referred in Figure 11. The corresponding displacements can be given by

$$u_x = \frac{p(1-v^2)}{\pi E}\left[\frac{1-2v}{1-v}\left[(x+a)\theta_1-(x-a)\theta_2\right]+2y\ln\frac{r_1}{r_2}\right] \tag{97}$$

$$u_y = \frac{p(1-v^2)}{\pi E}\left[\begin{array}{c}\dfrac{1-2v}{1-v}\left[y(\theta_1-\theta_2)+2H\arctan\dfrac{1}{c}\right]+2(x-a)\ln r_2 \\ -2(x+a)\ln r_1+4a\ln a+2a\ln(1+c^2)\end{array}\right] \tag{98}$$

where $H=ca$ is the distance from the origin to point $0'$, where the vertical displacement is assumed to be zero and c is a coefficient.

Owing to the symmetry about the y-axis, the problem is modeled with a $5a\times 5a$ square with $a=0.2\,\mathrm{m}$, $c=100$, and $p=1\,\mathrm{MPa}$. Other parameters are taken as $E=3.0\times 10^7\,\mathrm{Pa}$ and $v=0.3$. The left and bottom edges are constrained using exact displacement, while the right side is subjected to tractions computed from the analytical solutions.

The problem domain has been discretized with four models of node distributions (322, 651, 1252, and 2551 nodes, respectively) and the convergence rates for the displacement and energy norms are calculated using both LC-PIM and FEM. As shown in Figure 12, LC-PIM and FEM obtain similar accuracy and convergence rate for displacement calculation, but the former produces better accuracy and higher convergence rate for energy calculation than the latter. As we discussed previously, the convergence rate in energy norm of LC-PIM should be, theoretically, between 1.0 and 2.0. In this example, the convergence rate in energy norm is 0.98 (shown in Figure 12). The strain energy calculated based on numerical results has been plotted against the number of DOFs in Figure 13. It can be seen again that LC-PIM possesses the upper bound solution: strain energy of the LC-PIM solution is always larger than the exact one and converges to it with the increase in DOFs.

DOI: 10.1002/nme

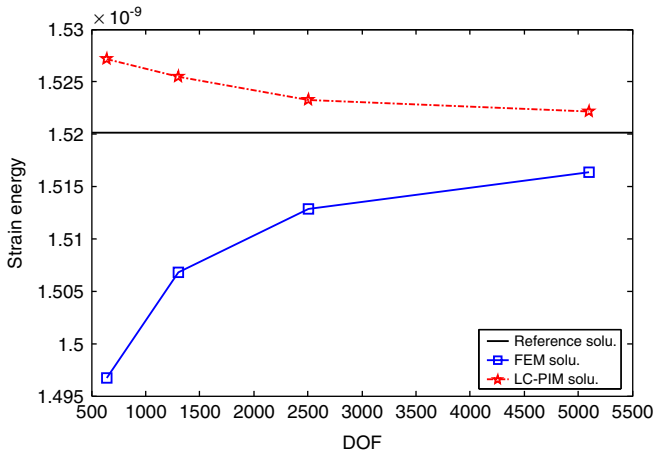

Figure 13. Upper bound solution obtained using the LC-PIM for the problem of 2D half space. The lower bound solution is obtained using the FEM using linear elements.

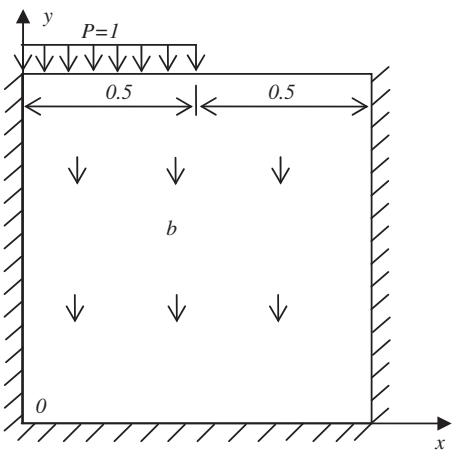

Figure 14. A square solid subjected to a uniform pressure.

6.5. *Square solid subjected to uniform pressure and body force*

A square solid shown in Figure 14 is now studied. The solids are constrained on the left, the right, and the bottom edges, and suffering from uniform pressure along the top edge and body force of $b^{\mathrm{T}}=\{0\ \ -1\}$. The problem is considered as plane stress with $E=3.0\times10^{7}$ Pa and $v=0.3$.

The problem is discretized with four models of 145, 313, 545, and 841 nodes, respectively. The property of upper bound on strain energy for LC-PIM is also investigated in similar ways as in the previous examples. As the analytical solution is not available for this problem, the reference solution of strain energy is obtained using the FEM with a very fine mesh (8238 nodes). The

DOI: 10.1002/nme

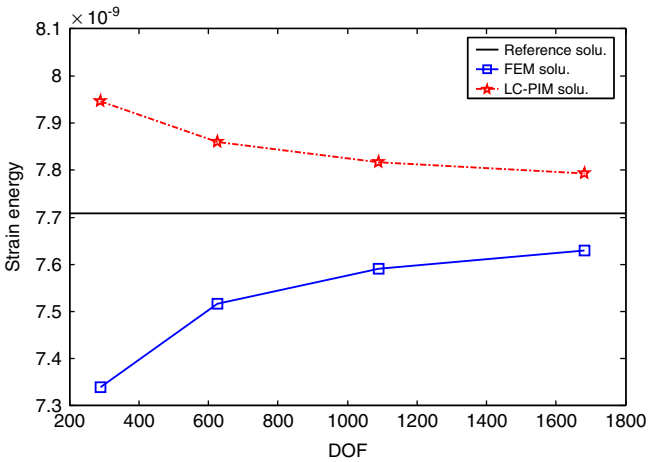

Figure 15. Upper bound solution obtained using the LC-PIM for the problem of square solid subjected to uniform pressure. The lower bound solution is obtained using the FEM using linear elements.

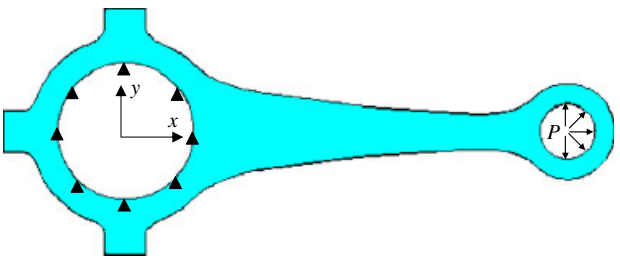

Figure 16. A connecting rod used in an automobile.

calculated strain energy has been plotted against the DOF in Figure 15. Again, LC-PIM gives the upper bound solution for this 2D problem.

6.6. An automotive part: connecting rod

A practical problem of typical connecting rod used in automobiles, as shown in Figure 16, is studied using LC-PIM. The rod is constrained along the left circle and subjected to a uniform radial pressure of 100 along the right circle as shown in the figure. The parameters are $E = 3.0 \times 10^7$ Pa and $v = 0.3$. As the exact solution is not available, a reference solution of strain energy is obtained using FEM with a very fine mesh (11226 nodes).

The problem is presented using four models of nodes distribution, i.e. 592, 1150, 1660, and 2244 nodes. The calculated strain energy has been plotted against the increase of DOFs in Figure 17. For this practical problem with complicated shape, the LC-PIM is found again to produce an upper bound solution in energy norm, while the FEM produces the lower bound.

DOI: 10.1002/nme

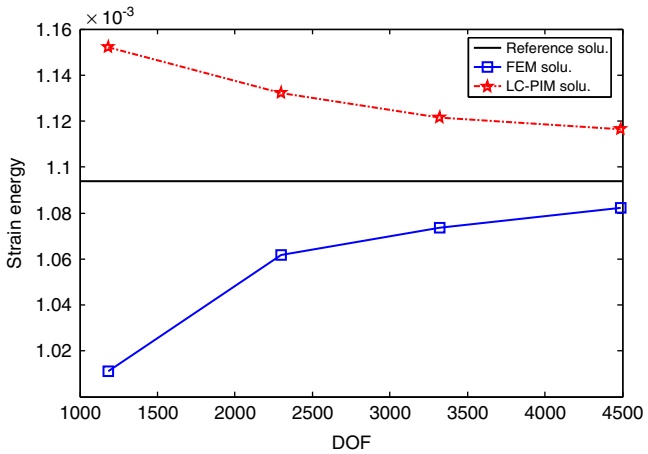

Figure 17. Upper bound solution obtained using the LC-PIM for the problem of connecting rod. The lower bound solution is obtained using the FEM using linear elements.

6.7. 3D Lame problem

A 3D Lame problem consists of a hollow sphere with inner radius a and outer radius b and subjected to internal pressure P, as shown in Figure 18. For this benchmark problem, the analytical solution is available in polar coordinate system [23]:

$$u_r = \frac{Pa^3 r}{E(b^3 - a^3)}\left[(1-2v) + (1+v)\frac{b^3}{2r^3}\right] \tag{99}$$

$$\sigma_r = \frac{Pa^3(b^3 - r^3)}{r^3(a^3 - b^3)} \tag{100}$$

$$\sigma_\theta = \frac{Pa^3(b^3 + 2r^3)}{2r^3(b^3 - a^3)} \tag{101}$$

where r is the radial distance between the centroid of the sphere and the point of interest in the sphere.

As the problem is spherically symmetrical, only one-eighth of the sphere is modeled and symmetry conditions are imposed on the three planes of symmetry. The numerical solution to this problem has been calculated using the material parameters $E = 1.0\,\text{Pa}$, $v = 0.3$, geometric parameters $a = 1\,\text{m}$, $b = 2\,\text{m}$, and internal pressure $P = 1\,\text{N/m}^2$.

The problem is discretized using four models of nodes distribution, i.e. 173, 317, 729, and 1304 nodes. The calculated strain energy has been plotted against the increase of DOFs in Figure 19 for both FEM and LC-PIM. For this 3D problem, LC-PIM is found again producing an upper bound solution, while the FEM produces the lower bound.

DOI: 10.1002/nme

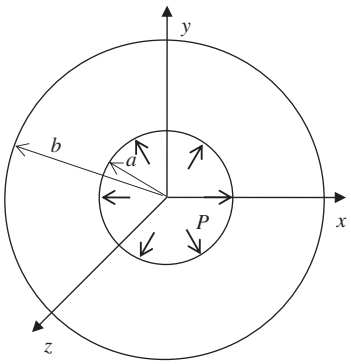

Figure 18. The 3D Lame problem of a hollow sphere subjected to an internal pressure.

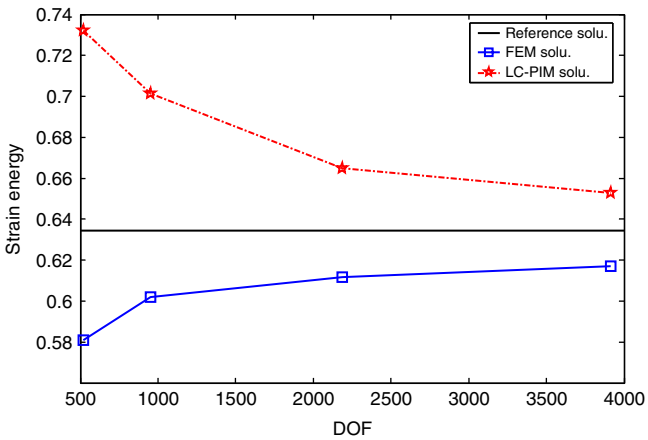

Figure 19. Upper bound solution obtained using the LC-PIM for the 3D Lame problem. The lower bound solution is obtained using the FEM using linear elements.

6.8. A 3D axletree base

Finally, a 3D practical problem of axletree base is studied using the present method. As shown in Figure 20, the axletree base is symmetric about the y–z plane, fixed in the locations of four lower cylindrical holes and subjected to a uniform pressure ($P = 100\,\mathrm{N/m^2}$) applied on the concave annulus. The parameters are taken as $E = 3.0 \times 10^7\,\mathrm{Pa}$ and $v = 0.3$.

The problem is presented using four models of 781, 1828, 2566, and 3675 nodes, respectively. The values of strain energy for both FEM and LC-PIM are plotted against the increase of DOF. As no analytical solution is available for this problem, a reference solution is obtained using the FEM with a very fine mesh (9963 nodes in total). Figure 21 shows that for this 3D practical problem with complicated shape, LC-PIM has again produced an upper bound solution: strain energy of LC-PIM solution is no less than the strain energy of the 'exact' solution and convergences to it with the increase in DOFs, while FEM solution convergences from below to the 'exact' solution.

DOI: 10.1002/nme

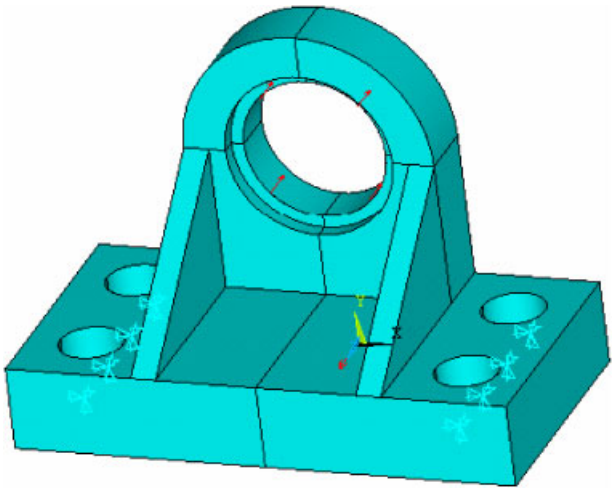

Figure 20. A 3D axletree base.

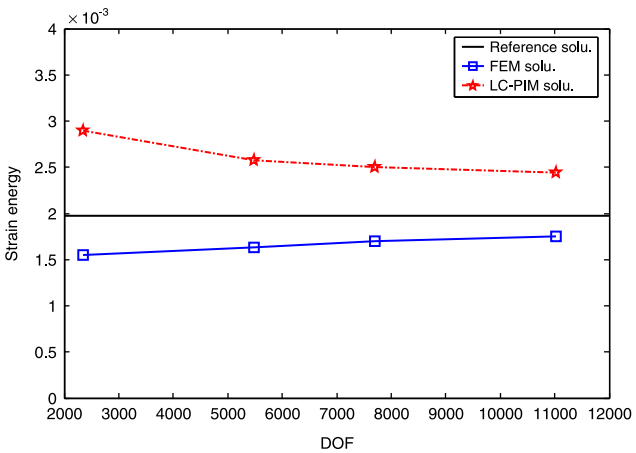

Figure 21. Upper bound solution obtained using the LC-PIM for the 3D axletree base problem. The lower bound solution is obtained using the FEM using linear elements.

7. EXTENSION

In the above theoretical and numerical studies, we used the same mesh for both LC-PIM and FEM models. In actual applications, there is no need to use the same mesh for these two methods, if our concerns are only on the solution bounds on the exact solutions. This is simply because we have found the bound properties of LC-PIM and FEM against, respectively, the exact solution. Therefore, for a given practical problem, we can use different meshes (if necessary), respectively, for LC-PIM and FEM, and the solutions of them will bound the exact solution from both above and below (except the trivial cases for LC-PIM). Using these bound properties of LC-PIM and

DOI: 10.1002/nme

FEM solutions, one can now effectively *certify* a numerical solution and conduct elegant *adaptive* analyses for solutions of *desired* accuracy.

8. CONCLUSION

In this work, a thorough theoretical study and an intensive numerical investigation on the linearly conforming point interpolation method (LC-PIM) have been conducted. We proved theoretically that

- The LC-PIM is variationally consistent, and the generalized Galerkin weak form is a valid weak form for generating the discretized system equations.
- The LC-PIM solution (in energy norm) is always no less than that of FEM.
- The LC-PIM solution (in energy norm) is no less than that of exact solution except a few trivial cases.

Intensive studies using 1D, 2D, and 3D problems have been then conducted, and we confirmed numerically that

- The LC-PIM solution (in energy norm) is always no less than that of FEM for all cases studied, without exception.
- The LC-PIM solution (in energy norm) is no less than that of exact solution except a few trivial cases: only one element is used, and the smoothing domain is reduced.
- Compared with the linear FEM, the LC-PIM gives similar accuracy and convergence rate for displacement calculation, but better accuracy and higher convergence rate in stresses.

We finally claim that using the LC-PIM together with the displacement-based fully compatible FEM model, we now have a systematical way to numerically obtain both upper and lower bounds of the exact solution to elasticity problems.

REFERENCES

1. Lucy LB. A numerical approach to testing the fission hypothesis. *The Astronomical Journal* 1977; **8**(12): 1013–1024.
2. Liu GR, Liu MB. *Smoothed Particle Hydrodynamics—A Meshfree Practical Method*. World Scientific: Singapore, 2003.
3. Nayroles B, Touzot G, Villon P. Generalizing the finite element method: diffuse approximation and diffuse elements. *Computational Mechanics* 1992; **10**:307–318.
4. Belytschko Y, Lu YY, Gu L. Element-free Galerkin methods. *International Journal for Numerical Methods in Engineering* 1994; **37**:229–256.
5. Liu WK, Jun S, Zhang YF. Reproducing kernel particle methods. *International Journal for Numerical Methods in Engineering* 1995; **20**:1081–1106.
6. Atluri SN, Zhu T. A new meshless local Petrov–Galerkin (MLPG) approach in computational mechanics. *Computational Mechanics* 1998; **22**:117–127.
7. Liu GR, Gu YT. A point interpolation method for two-dimensional solids. *International Journal for Numerical Methods in Engineering* 2001; **50**:937–951.
8. Wang JG, Liu GR. A point interpolation meshless method based on radial basis functions. *International Journal for Numerical Methods in Engineering* 2002; **54**:1623–1648.
9. Liu GR. *Meshfree methods*: *Moving Beyond the Finite Element Method*. CRC Press: Boca Raton, U.S.A., 2002.
10. Liu GR, Gu YT. *An Introduction to Meshfree Methods and Their Programming*. Springer: Dordrecht, The Netherlands, 2005.

DOI: 10.1002/nme

11. Liu GR, Zhang GY, Gu YT, Wang YY. A meshfree radial point interpolation method (RPIM) for three-dimensional solids. *Computational Mechanics* 2005; **36**(6):421–430.
12. Chen JS, Wu CT, Yoon S, You Y. A stabilized conforming nodal integration for Galerkin mesh-free methods. *International Journal for Numerical Methods in Engineering* 2001; **50**:435–466.
13. Liu GR, Li Y, Dai KY, Luan MY, Xue W. A linearly conforming RPIM for 2D solid mechanics. *International Journal of Computational Methods* 2006; **3**(4):401–428.
14. Liu GR, Zhang GY, Dai KY, Wang YY, Zhong ZH, Li GY, Han X. A linearly conforming point interpolation method (LC-PIM) for 2D solid mechanics problems. *International Journal of Computational Methods* 2005; **2**(4):645–665.
15. Zhang GY, Liu GR, Wang YY, Huang HT, Zhong ZH, Li GY, Han X. A linearly conforming point interpolation method (LC-PIM) for three-dimensional elasticity problems. *International Journal for Numerical Methods in Engineering* 2007; DOI: 10.1002/nme.2050.
16. Zienkiewicz OC, Taylor RL. *The Finite Element Method* (5th edn). Butterworth Heinemann: Oxford, U.K., 2000.
17. Liu GR, Quek SS. *The Finite Element Method: A Practical Course*. Butterworth Heinemann: Oxford, 2003.
18. Oliveira ER De AE. Theoretical foundations of the finite element method. *International Journal of Solids and Structures* 1968; **4**:929–952.
19. Wu HC. *Variational Principle in Elasticity and Applications.* Scientific Press: Beijing, 1982.
20. Simo JC, Hughes TJR. *Computational Inelasticity.* Springer: New York, 1998.
21. Liu GR, Dai KY, Nguyen TT. A smoothed finite element method for mechanics problems. *Computational Mechanics* 2007; **39**(6):859–877.
22. Liu GR, Nguyen TT, Dai KY, Lam KY. Theoretical aspects of the smoothed finite element method (SFEM). *International Journal for Numerical Methods in Engineering* 2007; **71**:902–930.
23. Timoshenko SP, Goodier JN. *Theory of Elasticity* (3rd edn). McGraw: New York, 1970.

DOI: 10.1002/nme